DEVELOPMENT OF A PROGRAMMABLE LOAD

Ulrich John Minnaar

A dissertation submitted to the Faculty of Engineering, University of the Witwatersrand, in fulfilment of the requirements for the degree of Master of Science in Engineering.

Johannesburg, 2006

DECLARATION

I declare that this dissertation is my own, unaided work. It is being submitted for the degree of Master of Science in the University of the Witwatersrand, Johannesburg. It has not been submitted before for any degree or examination in any other University.

_____

_____ day of _____ _____

ABSTRACT

The Voltage Dip Test Facility at the University of the Witwatersrand utilises a resistive load during testing of variable speed drives. This method produces valuable results regarding the performance of drives under dip conditions. It has been shown that load type does influence the performance of drives and this variation cannot be tested under current conditions as only linear loading is attainable with resistive loads. This thesis proposes a programmable load based on the concept of field-oriented control of an induction motor. The concepts involved with field-oriented control are discussed and shown to be suitable for this application. An implementation strategy utilising custom-designed software and an off-the-shelf VSD is developed and executed. The performance of the programmable load is analysed under both steady-state and dynamic conditions.

ACKNOWLEDGEMENTS

Thanks to SAFTRONICS for supplying the variable speed drive for the development work and Dr JM van Coller (Wits) for facilitating this. Thanks to Dr Van Coller for his guidance on the topic. Thanks also to Robert Koch for his comments. Further thanks to Harry Fellow and Indres Pillay (Wits workshop) for help with the mechanical and electrical set-up.

CONTENTS **Page**

LIST OF FIGURES

Figure **Page**

LIST OF TABLES

Table **Page**

NOMENCLATURE

AC	Alternating Current
A/D	Analogue To Digital
ASD	Adjustable Speed Drive
D/A	Digital To Analogue
DC	Direct Current
LV	Low Voltage
EPRI	Electric Power Research Institute
EMC	Electromagnetic Compatibility
HV	High Voltage
IEEE	Institute Of Electrical And Electronic Engineers
IGBT	Insulated Gate Bipolar Transistor
LED	Light Emitting Diode
LV	Low Voltage
MV	Medium Voltage
PC	Personal Computer
PLC	Programmable Logic Controller
PQ	Power Quality
PWM	Pulse Width Modulation
R.M.S	Root Mean Squared
SLGF	Single-Line-To-Ground fault
VSD	Variable Speed Drive

1. INTRODUCTION

1.1 PROBLEM STATEMENT

Voltage dips are estimated to cost South African industry approximately R1.2 billion rands [1]. This cost is due to production losses caused by the tripping of plant equipment. A solution to this problem can only be sought once the behaviour of equipment under voltage dip conditions is understood.

The Power Quality Test Laboratory (PQ Test Lab) is the result of collaboration between the University of the Witwatersrand and Eskom-TSI. The PQ Test Lab was originally developed to investigate the response of variable speed drives under voltage dip conditions. The capability of the laboratory has been extended to include the testing of auxiliary plant equipment e.g. contactors, relays, pc power supplies.

The PQ Testlab utilises a developed methodology to obtain information regarding the impact of voltage dips on the above-mentioned equipment and provides a valuable input to industry regarding equipment sensitivity.

The aim of the laboratory is to facilitate power quality investigations and system compatibility studies. The aim of system compatibility studies is to render industry insensitive to the effects of supply disturbances by either rigorous equipment specification or the implementation of remedial solutions on existing equipment [2].

At present testing is done under resistive load conditions. This methodology produces valuable generic information regarding the response of equipment to voltage dips, however it has been shown that variable speed drives have varying responses to voltage dips determined by load type [3].

This report investigates the various load type scenarios present in industry and proposes the use of a programmable load to simulate

industrial conditions in the laboratory. A load topology is proposed with supporting theory.

The introduction of a programmable load to the PQ Testlab will enhance the ability of the laboratory to measure the response of variable speed drives under a range of conditions related to voltage dip and load type variations.

2. BACKGROUND

2.1 Voltage Dips

Voltage dips are also referred to as voltage sags, most notably in the USA. Figure 1 indicates the difference in definition between dip magnitude and sag magnitude. Voltage dip and dip magnitude will be referred to in this document, unless otherwise stated.

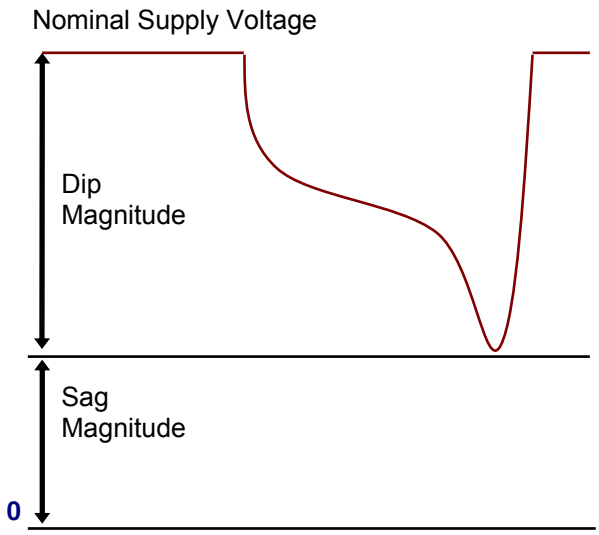

Figure 1: Difference between sag and dip magnitude [4]

A voltage dip is defined by NRS-048, the South African regulatory standard governing quality of supply as:

"A sudden reduction in the r.m.s. voltage, for a period between 20ms and 3 s, of any or all of the phase voltages of a single-phase or a polyphase supply. The duration of a voltage dip is the time measured from the moment the r.m.s voltage drops below 0.9 per unit of declared voltage to when the voltage rises above 0.9 per unit of declared voltage." Here the declared voltage is defined as "The voltage declared by the utility as the voltage at the point of supply." This is illustrated in Figure 2.

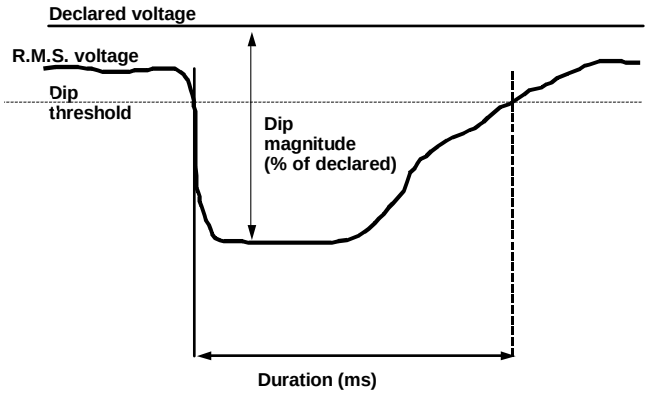

Figure 2: Measured voltage dip parameters [6]

The characterisation of voltage dips in terms of magnitude and duration provides the essential information for the quantification of voltage dips [4]. This information however does not adequately explain all effects of voltage dips on equipment [2]. Voltage dips can also be represented by means of r.m.s values and phasor diagrams. Using phasor diagrams, three types of voltage dips are described: three-phase dips, single-phase dips and phase-to-phase voltage dips. These are illustrated in figure 3.

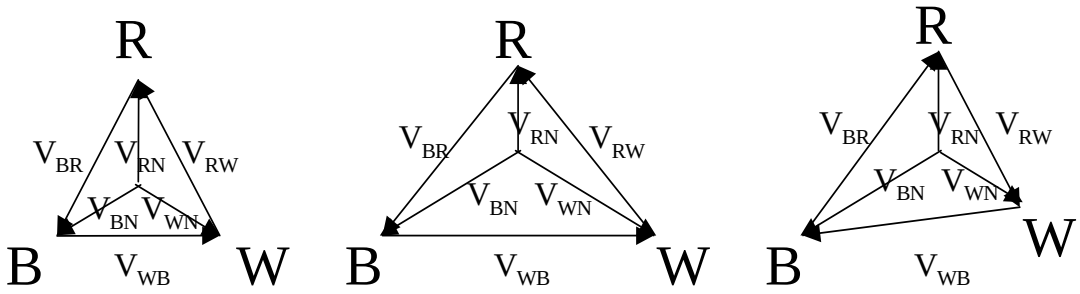

(a) Three-phase dip **(b) Single-phase dip** **(c) Phase-to-phase dip**

Figure 3: The three basic voltage dip types [2]

Voltage dips are further described in IEEE 1159.2 [7] according to the following list of descriptors.

- RMS magnitude
- Duration
- Point-in-wave of initiation
- Point-in-wave of recovery
- Phase shift
- Rate of change of phase shift
- Missing voltage

The relationship between the three phases is also important to many types of industrial equipment as they may operate off the difference between two phases. The phase shift between two phases is then critical. This is case when considering drives and their performance under voltage disturbances. The three phase situation is described by:

- R.M.S magnitude unbalance ratio
- Difference voltage
- Phase angle relationship

This information provides specific insight into voltage disturbance waveforms and allows engineers to determine the reason for equipment mal-operation at specific sights. This data can also be used to better design equipment to deal with normal power system disturbances [4].

2.2 Effects of Voltage Dips on Variable Speed Drives

A typical AC pulse width modulated (PWM) drive consists of three stages namely:

A rectifier stage converting incoming AC voltage to DC voltage, a DC bus storing energy and minimising voltage ripple as well the inverter stage that converts DC to an AC voltage of the required magnitude and frequency using PWM.

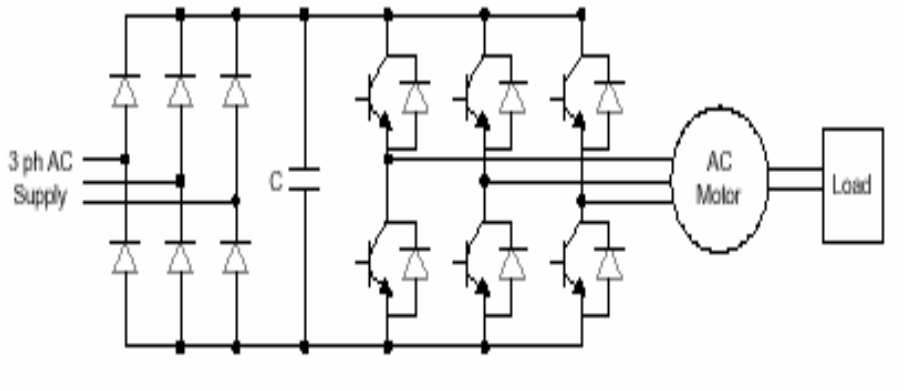

Figure 4: Typical AC Drive Topology [8]

AC drives normally utilise an uncontrolled rectifier stage and the capacitor in the DC link provides some measure of energy storage which assists in voltage dip ride-through of AC drives, most AC drives are however very sensitive to voltage dips.

The DC bus voltage decreases during a voltage dip. When this voltage reaches the under-voltage trip point, the drive will trip on undervoltage [9].

The uncontrolled rectifier stage of the drive does not require timing information from the rectifier and ignores zero crossings. This means

that the phase shifts during voltage dips does not significantly affect the performance of AC PWM drives [10].

The majority of voltage dips are due to single-line-to-ground-faults (SLGF) [10]. During a SLGF the voltage on the faulted phase goes to zero volts at the location of the fault. The voltage at a customer busbar is influenced by fault type, fault impedance, distance to customer busbar and transformer connections etc. [4, 10].

Table 1 [4] shows phase voltage magnitudes on a transformer secondary during a SLGF. The fault occurred on phase A.

Transformer connection	Line voltages on the transformer secondary		
	Vab	Vbc	Vca
Y/Y	0.58	1.0	0.58
D/D	0.58	1.0	0.58
Y/D	0.33	0.88	0.88
D/Y	0.88	0.88	0.33

Table 1: Phase voltage magnitude during SLGF on phase A [4]

Voltage unbalance created during such dips may cause tripping of the drive.

The input rectifier draws current when the phase voltage exceeds the DC bus capacitor voltage. For a balanced input voltage supply the line current waveforms are typically as in Figure 5, which is for a 5hp (3,75KW) AC drive.

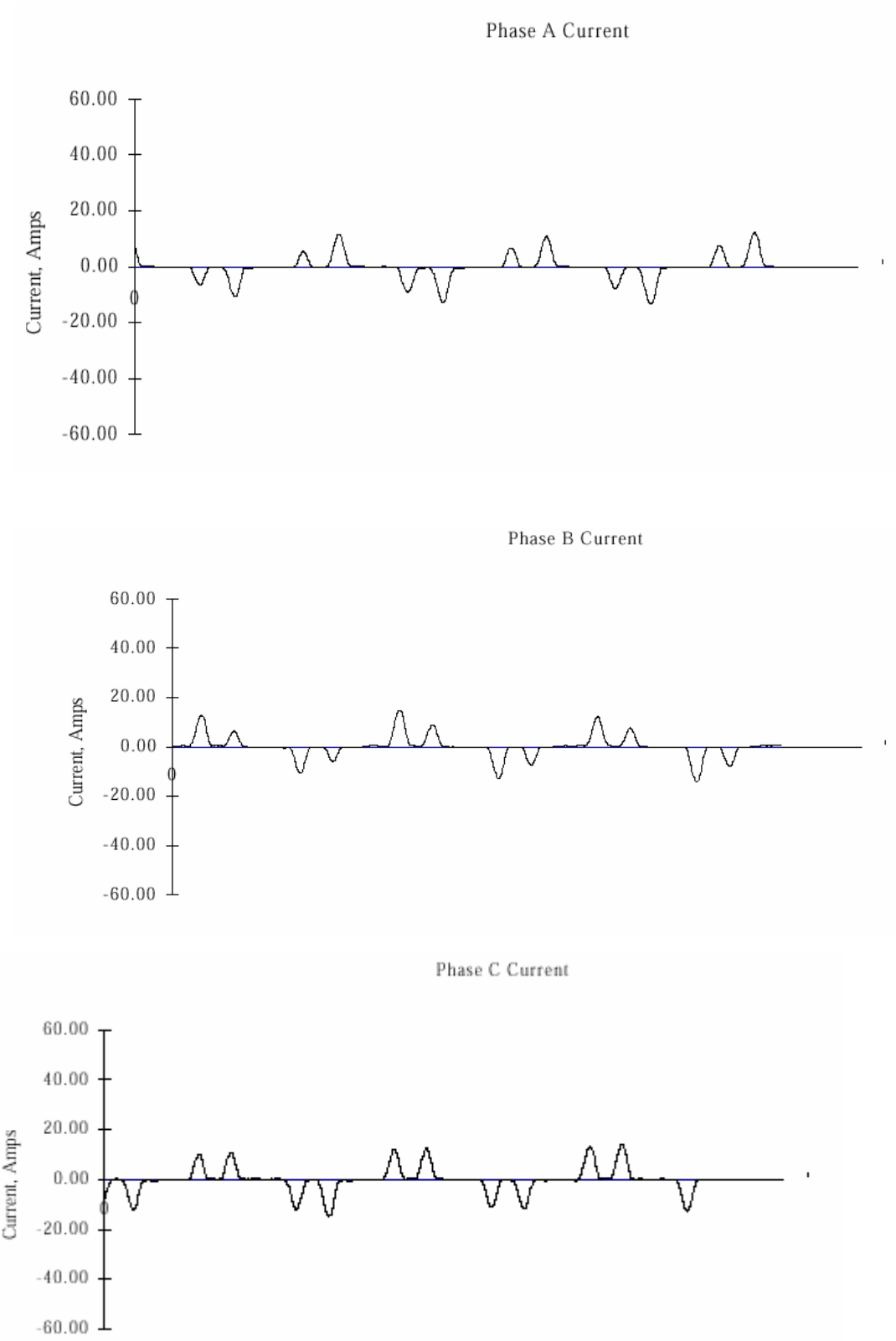

Figure 5: Lines currents for balanced voltage supply [10]

For unbalanced phase voltages such as those occurring during SLGF`s the input current may be in excess of 200% of the normal rating and peak current drawn may be 4 times the normal [10]. These large currents exist due to the capacitor not drawing current from the dipped phase that is under the DC bus voltage; hence the capacitor discharges more stored energy to the motor and load. When the phase that has not dipped forward biases the rectifier, the capacitor is recharged from this line causing large currents to flow in the line. AC drives commonly trip due to undervoltage on a set threshold or overcurrent caused by high line currents [10].

Figure 6 indicates the line currents drawn on a 3% voltage unbalance for the same AC drive illustrated in Figure 5.

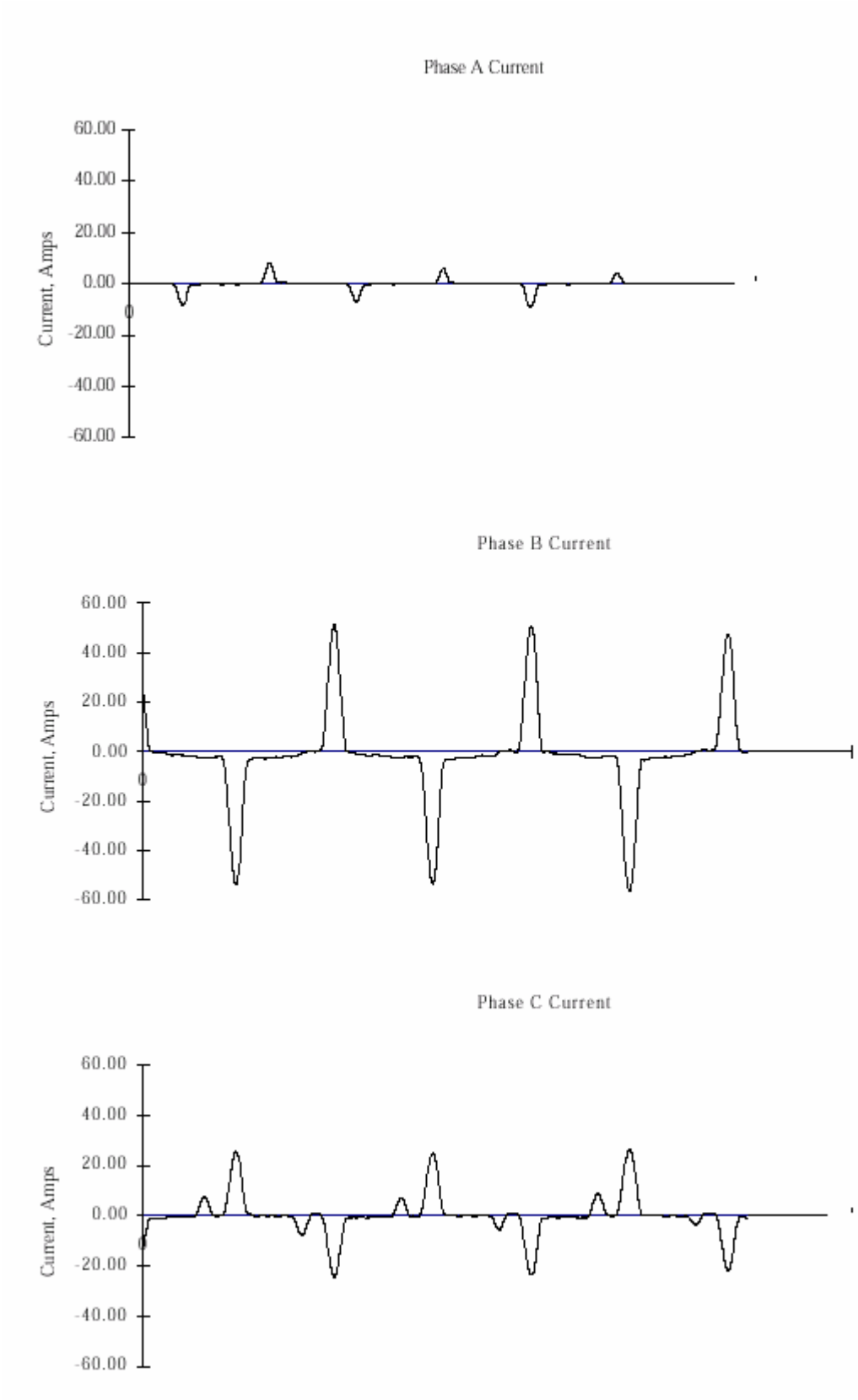

Figure 6: Line currents for 3% voltage unbalance [10]

3. THE EFFECT OF LOAD CHARACTERISTICS ON VSD PERFORMANCE

To understand the effects of load on VSD performance a good starting point is the application of the load in an industrial situation i.e. the driving of a load by an electric motor.

An electrical motor converts electrical energy into rotational mechanical energy. The rotor shaft spins at a specific speed with the requirement to turn or move a device. This device is the load and a certain amount of force is required to initiate movement of the load and to maintain this movement. This will determine the characteristic of the load.

There are three terms of importance when characterising electric motor loading: torque, speed and inertia [11].

- **Torque** is defined as the mechanical force multiplied by vertical distance (lever arm) [12]. It is a measure of how much force is required to cause an object to rotate i.e. the load. The metric unit for torque is Nm.

- **Speed** is the rotational velocity of the driving shaft. It is measured in R.P.M (revolutions per minute). Also measured as ω(omega) with unit radians per second.

- **Inertia** is the tendency of an object to resist any change in motion. Mass is used to measure inertia.

Two condition states have to be considered for analysis of Load type. These are steady state conditions and dynamic conditions. Steady state conditions mean that the load is not undergoing acceleration or deceleration. Torque and speed are plotted against each other to give a representation of the steady-state torque requirements of the load throughout its speed range.

The steady-state torque-speed curve can normally be fitted to a mathematical equation relating torque to speed [11].

$$T_L = \sum_{n=-\infty}^{\infty} A_n \omega_m^n$$

Industrial loads generally fit into three load type categories: constant torque, constant power and variable torque loads [11]

3.1 Constant Torque

Constant torque loads have torque requirements that are independent of speed. The torque requirement remains the same throughout the speed range of the system.

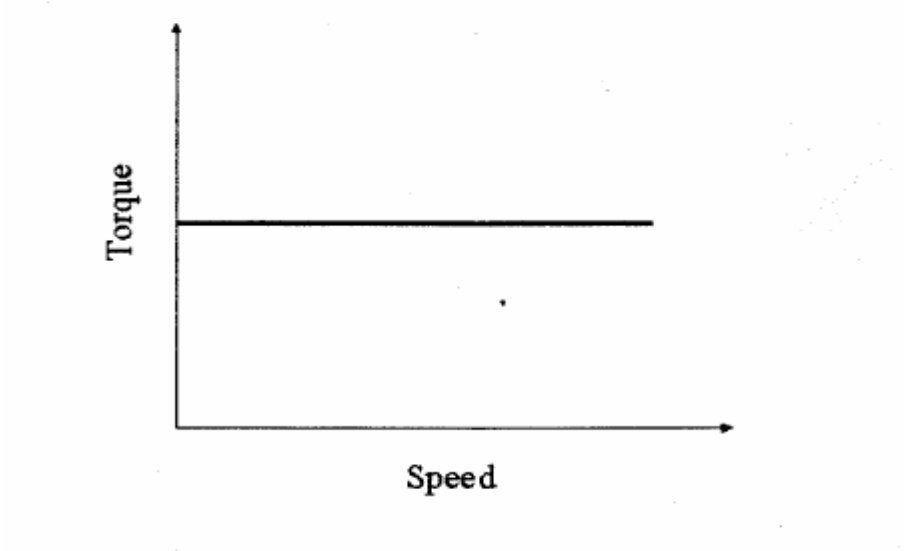

Figure 7: Torque-speed Characteristic for Constant-Torque Load [11]

Figure 7 illustrates the characteristic curve for constant torque loads and it is important to note that full torque is required at zero speed. Examples of constant torque loads include conveyors, extruders and positive displacement pumps [11, 13].

The steady-state equation governing this load-type is:

$$T_L = A_0 \text{.....(1)}$$

3.2 Constant Power

The equation defining rotational power [12] is:

$$P = T \times \omega_m \quad \text{.....} \quad (2)$$

Where: P = power

T = torque

ω_m= angular speed

Equation (1) indicates that for any constant value of power, torque decreases as speed increases and vice versa. Figure 8 shows the characteristic curve for this load-type.

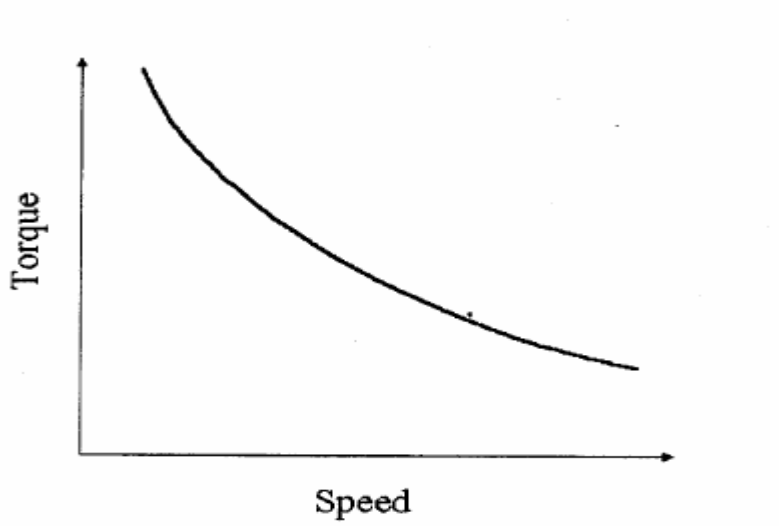

Figure 8: Torque-Speed Characteristic for Constant-Power Load [11]

Equation (1) is of the form of a hyperbolic function and the torque-speed curve is therefore inherently of this form. Figure 8 indicates that the highest required torque is reached at low speeds. Examples include traction motors, cranes, lathes and centre winders [11].

3.3 Variable Torque

Variable torque loads in general follow a quadratic torque-speed [11] curve of the form:

$$T_L(\omega) = A_2\omega_m^2 + A_1\omega_m + A_0 \quad \text{.....} \quad (3)$$

Where: T_L = load torque

ω_m = angular speed

A_0= constant

Every load has a particular set of co-efficients that describe how load torque varies with speed. Examples include fans, blowers, centrifugal pumps, and compressors [11]. The torque-speed characteristic is typically as in figure 9.

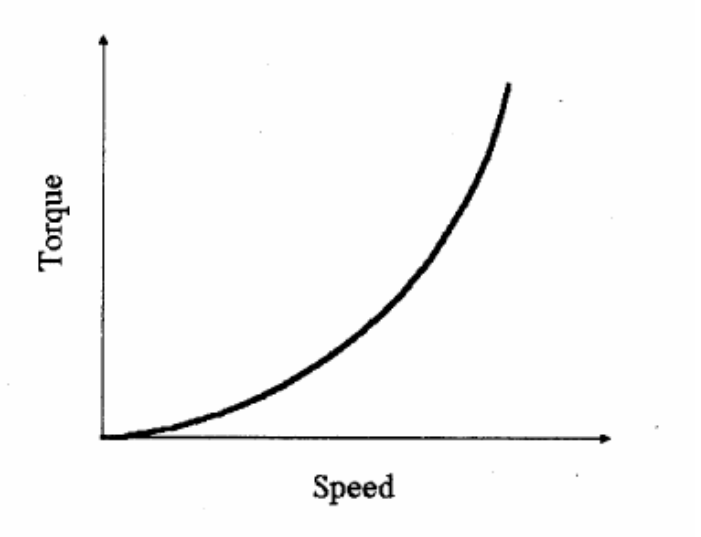

Figure 9: Torque-Speed Characteristic for Variable-Torque Load [11]

Figure 9 illustrates the relationship between torque and speed. This figure points out the variation of torque with respect to speed.

Although the exact curve for variable torque loads are highly dependent on specific applications, the following generalisation can be used as a guideline for describing variable torque loads.

$$T \propto \omega^2 .....(3)$$

The curve for variable torque loads can therefore be approximated by:

$$T_L = A_2 \omega_m^2 .....(4)$$

The three load types mentioned above cover a range of engineering applications. Table 2 provides a list of applications specific to each load type.

LOAD TYPE	CHARACTERISTIC CURVE	APPLICATIONS
CONSTANT TORQUE	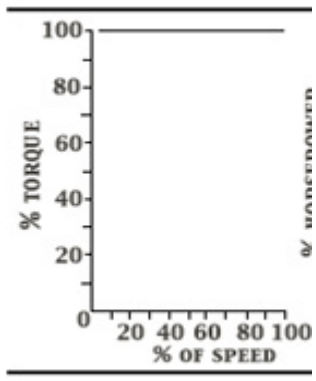	-conveyors, extruders, mills, planers, screw pumps, piston pumps, lifts, winders, positive displacement pumps
CONSTANT POWER	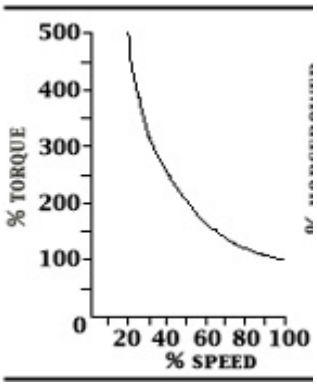	-traction motors, cranes, lathes, centre winders
VARIABLE TORQUE (Quadratic function)	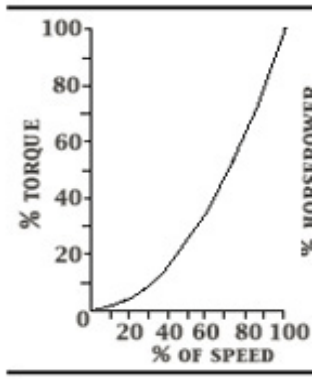	- blowers, centrifugal fans, centrifugal pumps, vacuum pumps, compressors

Table 2: Examples of load type applications [11, 13]

3.4 Dynamic Conditions

Steady–state conditions and load inertia are used to describe the dynamic load torque resulting from acceleration or deceleration [11].

Newton's Second Law states: *"The relationship between an object's mass m, its acceleration a, and the applied force F is F = ma"* [12].

For rotational systems this means that loads with high inertia will create a torque in opposition to the system speed. It follows then that the magnitude of the load inertia will affect the drive performance. Larger inertia values will mean more stored mechanical energy that will keep a system rotating during a voltage dip. A load is described as having a high inertia if the load inertia is more than 5 times the motor inertia [13].

The equation governing dynamic torque conditions is:

$$T_L = J_L \frac{d\omega_m}{dt} + \sum_{n=-\infty}^{\infty} A_n \omega_m \text{.....(5)}$$

This equation comprises an inertia component and a steady-state component, which is system dependent as described previously.

3.5 Impact of load types under dip conditions

EPRI have developed a 5-HP programmable load and tests conducted using this load indicate that speed and torque changes that take place during voltage dips differ for various load types. [11]

Tests were conducted on quadratic, constant power and constant torque load types. Three phase voltages dips up to 30% of nominal were applied to the input of the drive under test. The tests were carried out with a flying restart enabled. The initial conditions for the test was **speed = 1740RPM** and **load torque = 20.5 Nm**. [11].

The dips were applied at 5, 10, 15, 20, 25 and 30 cycles. Figure 10 and 11 use voltage sags as opposed to voltage dips.

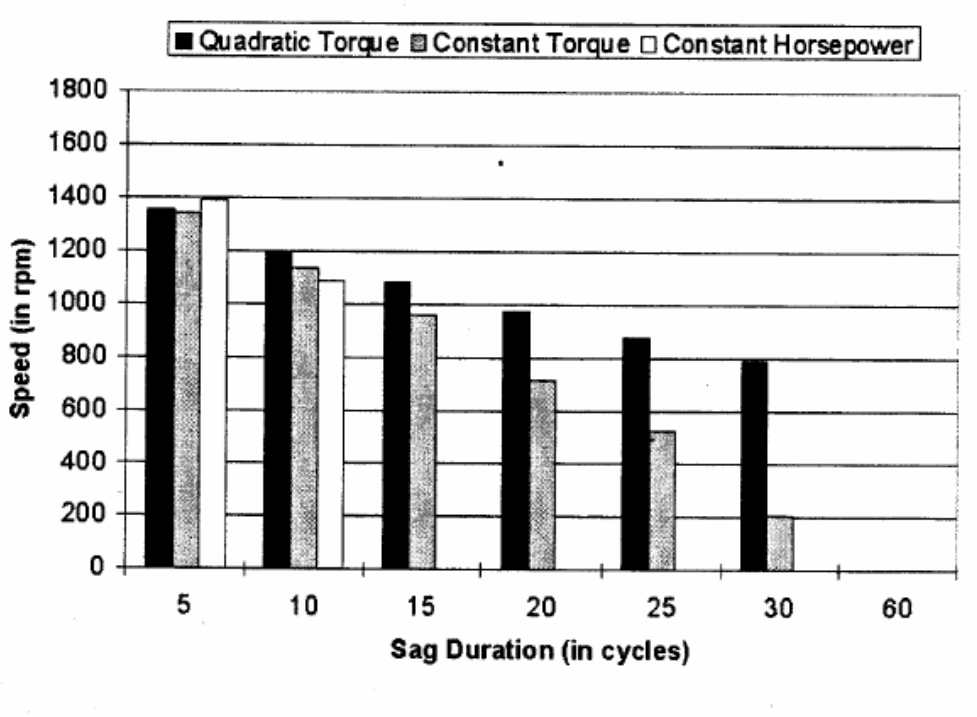

Figure 10: Speed vs. Dip duration for 3 load types [11]

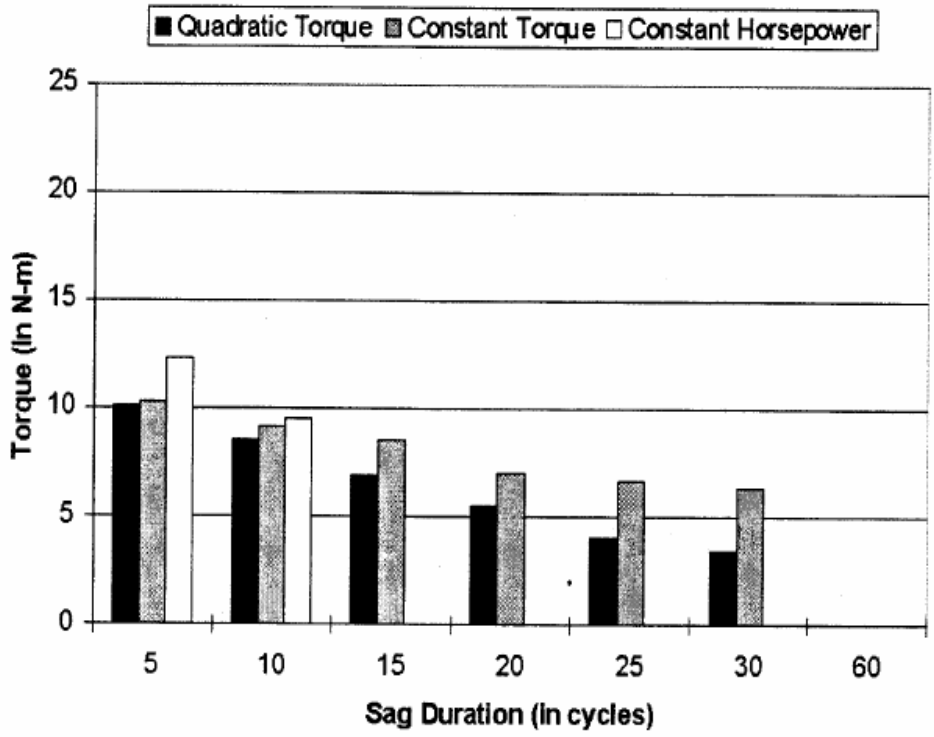

Figure 11: Torque vs. Dip duration [11]

The results indicate that both load type and dip duration has a significant effect on the on speed and torque changes. Figures 10 and 11 show that different load types produce different torque and speed changes for identical voltage dips. The unique response of each load type to voltage dips indicates that load type needs to be taken into consideration when voltage dip testing takes place as it could significantly affect drive performance and ride-through ability.

4. THE VOLTAGE DIP TEST FACILITY

The Power Quality Test Facility (PQ Test Lab) is located at the University of the Witwatersrand and was originally designed to provide a dip immunity testing facility for variable speed drives. The facility has been expanded to include voltage dip testing of auxiliary equipment such as contactors, relays, programmable logic controllers and pc power supplies.

The voltage dip testbed consists of the following [15]:

- A supply control PC
- Input (A/D) and output (D/A) interface cards
- A programmable supply incorporating an IGBT output inverter stage, supplied via three-phase rectifier
- An output transformer
- An induction motor coupled to a DC generator
- A variac/rectifier to adjust the generator field
- A resistor bank serving as the generator load

4.1 The Layout of the Test Facility

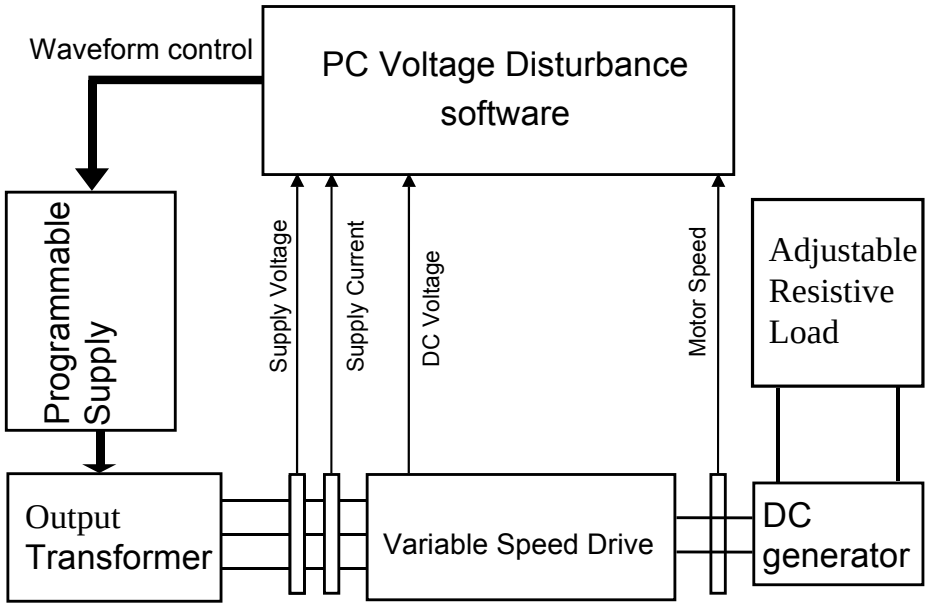

Figure 12: Block diagram of the voltage dip test-bed [2]

A PC is used to synthesise a voltage dip by specifying voltage dip parameters such as the voltage prior to the voltage dip, the voltage during the voltage dip, the phase angle and the voltage recovery profile. Parameters can be adjusted independently for each of the phases such that single-phase, two-phase and three-phase voltage dips can be tested.

The test facility, shown in Figure 12, consists of the following elements [2]:

- The PC, running the dip testing software, is used to control the testing. The voltage dip software controls the pre-dip waveform generation and voltage dip generation by the programmable supply. During and immediately after an applied voltage dip, VSD measurements are recorded for analysis after the test.

- The programmable supply replaces the mains supply to the equipment. The programmable supply is IGBT based and, with the controller that was developed, is capable of generating any complex voltage dip waveform.

- The VSI or CSI inverter is connected to a standard induction motor, which in turn is coupled to a DC generator load.

- The DC generator, which is coupled to the induction motor, is connected to a resistive load bank. By adjusting the generator field current the load presented by the DC generator is varied. With constant field and resistive load the DC generator load presents a linear torque versus speed characteristic.

The voltage dip test facility in its present form provides a valuable tool in performing dip immunity testing of variable speed drives. It has, however been shown in the previous chapter that load characteristic plays a role in the performance of drives under voltage dip conditions. The present

load utilised in the laboratory does not compensate for variation in load type and presents a linear torque-speed curve.

This report proposes replacing the current resistive load with a programmable load that is capable of generating the required torque speed characteristics and simulating dynamic torque conditions. Figure 13 illustrates the proposed system layout.

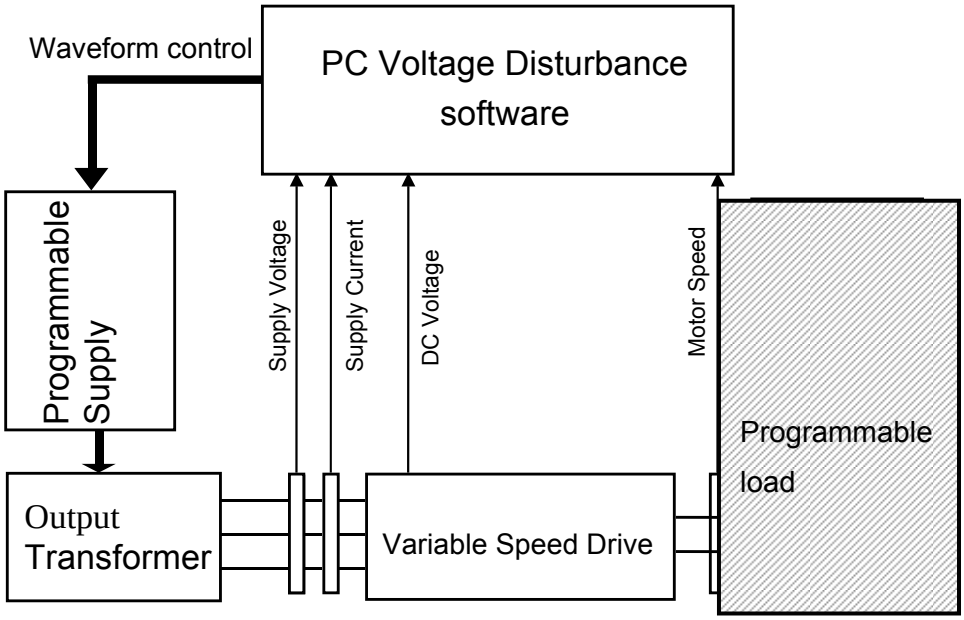

Figure 13: Proposed layout

5. PROGRAMMABLE LOAD

5.1 Load Requirements

The function of the programmable load will be to simulate typical industrial loads as described previously.
This will include:

- Maximum torque at zero speed
- Simulate inertia effects under deceleration and acceleration
- Quick response to changes in ω (angular velocity) via feedback

The implementation of the load involves the application of an opposing torque simulating both steady state and dynamic conditions. This limits the control schemes that are applicable for this instance. This report proposes utilising and induction motor to provide the opposing torque simulating the load.

Classical AC drives are limited in their ability to fulfil this function for the following reasons [16]:

- The machine models and characteristics are only valid for steady state
- No 3-phase imbalance management as there is no consideration of phase interactions.
- Difficulty controlling variables with a sinusoidal reference.
- Control structure Must be dedicated to a specific motor type i.e. synchronous or asynchronous

Field oriented control offers accurate control for both steady state and dynamic conditions as it incorporates exact motor transient equations.

Field oriented control consists of controlling the stator currents represented by a vector. It is based on projections that transform a three-phase time and speed dependent system into a two state time invariant system. As field control is based in projections, the control structures handle instantaneous electrical quantities. This means that

the control is accurate in every working instance, both steady state and instantaneous.

An understanding of space vector theory of AC motors is required before moving into field-oriented control theory.

5.2 Space Vector Theory of AC Motors

In space vector theory the actual winding currents are replaced with equivalent rotating current space vectors. These in turn produce rotating flux space vectors that induce voltages in the windings. The winding voltages are also replaced with voltage space vectors.

Stator voltage equation in space vector form is:

$$\vec{v}_S(t) = \vec{i}_S(t)R_S + \frac{d\vec{\psi}_S(t)}{dt} \quad \text{.....(7)}$$

Where $\vec{v}_S(t)$ is the rotating stator voltage space vector

$\vec{i}_S(t)$ is the rotting stator current space vector

R_S is the stator winding resistance

$\vec{\psi}_S(t)$ is the rotating stator flux linkage space vector

Similarly the **rotor voltage equation** is:

$$\vec{v}_R(t) = \vec{i}_R(t)R_R + \frac{d\vec{\psi}_R(t)}{dt} \quad \text{.....(8)}$$

Where $\vec{v}_R(t)$ is the rotating rotor voltage equation

$\vec{i}_R(t)$ is the rotating rotor current space vector

R_R is the rotor winding resistance

$\vec{\psi}_R(t)$ is the rotating rotor flux linkage space vector

5.2.1 Generalised Voltage Space Vector Equations

Assume a 2-pole motor with 3-hase windings on stator and rotor.

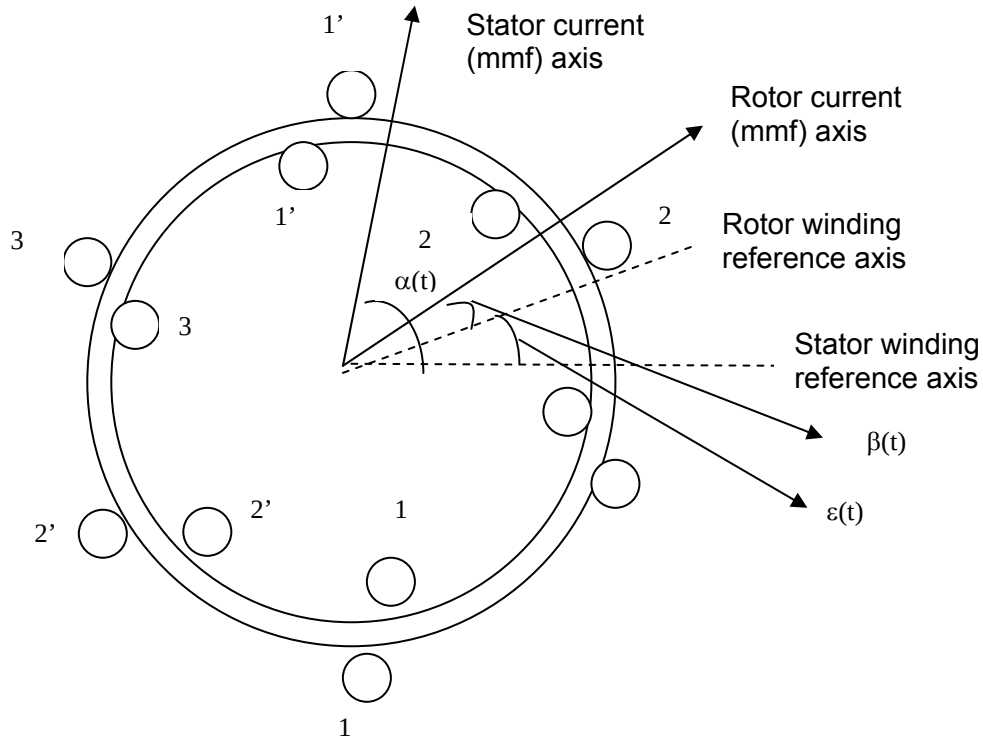

Figure 14: Representation 2 pole 3-phase AC induction motor

Define: the stator winding reference axis as the axis of stator phase 1 winding

the rotor winding reference axis as the axis of rotor phase 1 winding

$i_{S1}(t)$ as the **instantaneous** current in phase 1 winding

$i_{S2}(t)$ as the **instantaneous** current in phase 2 winding

$i_{S3}(t)$ as the **instantaneous** current in phase 3 winding

From this the **stator current space vector (**referenced to the **stator winding reference axis)** is defined as:

$$\vec{i}_S^{\,s}(t) = i_S(t)e^{j\alpha(t)} = i_{S1}(t)e^{j0} + i_{S2}(t)e^{j2\pi/3} + i_{S2}(t)e^{j4\pi/3} \quad ..(9)$$

Where: $i_S(t)$ is the magnitude of the stator current space vector as a function of time

α(t) is the angle of the stator current space vector as a function of time

- The actual winding currents are considered to produce stationary current space vectors which when added together produce a rotating current space vector
- The angular separation of the stationery current space vectors are a result of the physical separation of the windings
- Balanced 3-phase currents cause $i^s_S(t)$ to rotate with constant angular velocity and constant magnitude, for all other cases angular velocity and magnitude are not constant

We define the **stator mmf space vector** (also referenced to the **stator winding reference axis**) as:

$$\vec{F}_S^{\,s}(t) = N_S i_S^s(t) = N_S i_S(t) e^{j\alpha(t)} = F_S(t) e^{j\alpha(t)} .....(10)$$

where: N_S is the number of turns per phase on the stator windings

F_s is the magnitude of the stator space windings

α(t) is the angle of the stator mmf space vector

Similarly the **rotor current space vector** (referenced to the rotor winding reference axis) is:

$$\vec{i}_R^{\,r}(t) = i_R(t) e^{j\beta(t)} = i_{R1}(t) e^{j0} + i_{R2}(t) e^{j2\pi/3} + i_{R2}(t) e^{j4\pi/3} .....(11)$$

Which produces a **rotor mmf space vector** (referenced to the rotor winding reference axis)

$$\vec{F}_R^{\,r}(t) = N_R i_R^r(t) = N_R i_R(t) e^{j\beta(t)} = F_R(t) e^{j\beta(t)} .....(12)$$

where: N_R is the number of turns per phase on the rotor windings

F_R is the magnitude of the rotor space windings

β(t) is the angle of the rotor mmf space vector

Assuming iron has zero reluctance, the total mmf is dropped across the two air gaps. It can be shown that the above mmf space vectors (rotor and stator) together produce the following flux density space vectors [17].

Stator flux density space vector

$$\vec{B}_S^s(t) = \frac{\mu_0}{2h}\left[\vec{F}_S^s(t) + \aleph\vec{F}_R^s(t)\right].....(13)$$

Rotor flux density space vector

$$\vec{B}_R^r(t) = \frac{\mu_0}{2h}\left[\aleph\,\vec{F}_S^r(t) + \vec{F}_R^r(t)\right].....(14)$$

where: $B_S(t)$ is the magnitude of the stator flux density space vector

$B_R(t)$ is the magnitude of the rotor flux density space vector

$\aleph$ is coupling factor dependent on leakage ($0 \le \aleph \le 1$)

μ_0 is the permeability of air

h is the air gap length

The stator flux density space vector gives rise to flux linkage in each of the 3 phase windings. When these 3 flux linkages are vectorially added they produce the **stator flux linkage space vector:**

$$\vec{\psi}_S^s(t) = \frac{3rlN_S\pi}{4}\vec{B}_S^s(t).....(15)$$

where r is the radius of the stator winding

l is the axial length of the rotor

Equation 15 shows that the stator flux linkage vector space vector is related to the stator flux density space vector by a constant of proportionality. Substituting equation 13 into equation 15.

$$\vec{\psi}_S^s(t) = \frac{3\mu_0 rlN_S^2\pi}{8h}\vec{i}_S^{\,s}(t) + \frac{3\mu_0 rlN_S N_R\pi}{8h} i_R^r(t)e^{j\varepsilon(t)} \quad \text{.....(16)}$$

The term $\frac{3\mu_0 rlN_S^2\pi}{8h}$ has the form of **self-inductance of the stator winding** and is denoted by L_S, while $\frac{3\mu_0 rlN_S N_R\pi}{8h}$ has the form of mutual inductance of stator and rotor windings and is denoted by M.

Then:

$$\psi_S^s(t) = L_S\vec{i}_S^{\,s}(t) + M\vec{i}_R^{\,r}(t)e^{j\varepsilon(t)} \quad \text{.....(17)}$$

Similarly for the rotor $L_R = \frac{3\mu_0 rlN_R^2\pi}{8h}$ is the **self-inductance of the rotor winding,** and the **rotor flux linkage space vector** is:

$$\vec{\psi}_R^r(t) = L_R\vec{i}_R^{\,r}(t) + M\vec{i}_S^{\,s}(t)e^{-j\varepsilon(t)} \quad \text{.....(18)}$$

It is now possible to relate the current space vectors and the voltage space vectors in terms of resistances, self and mutual inductances. Substituting into Equation 7 we get Equation 19, the **stator voltage space vector**:

$$\vec{v}_S^s(t) = R_S\vec{i}_S^s(t) + \frac{d}{dt}\vec{\psi}_S^s(t)$$

$$= R_S\vec{i}_S^s(t) + L_S\frac{d}{dt}\vec{i}_S^s(t) + M\frac{d}{dt}\left[\vec{i}_R^r(t)e^{j\varepsilon(t)}\right]$$

$$= R_S\vec{i}_S^s(t) + L_S\left[\frac{d}{dt}i_S(t)\right]e^{j\alpha(t)} + jL_S\left[\frac{d\alpha(t)}{dt}\right]i_S(t)e^{j\alpha(t)}$$

$$+ M\left[\frac{d}{dt}i_R(t)\right]e^{j(\beta(t)+\varepsilon(t))} + jM\left[\frac{d(\beta(t)+\varepsilon(t))}{dt}\right]i_R(t)e^{j(\beta(t)+\varepsilon(t))}$$

Similarly from equation 8, we get the **rotor voltage space vector (equation 20)**:

$$\vec{v}_R^r(t) = R_R\vec{i}_R^r(t) + \frac{d}{dt}\vec{\psi}_R^r(t)$$

$$= R_R\vec{i}_R^r(t) + L_R\frac{d}{dt}\vec{i}_R^r(t) + M\frac{d}{dt}\left[\vec{i}_S^s(t)e^{-j\varepsilon(t)}\right]$$

$$= R_R\vec{i}_R^r(t) + L_R\left[\frac{d}{dt}i_R(t)\right]e^{j\beta(t)} + jL_R\left[\frac{d\beta(t)}{dt}\right]i_Re^{j\beta(t)}$$

$$+ M\left[\frac{d}{dt}i_S(t)\right]e^{j(\alpha(t)-\varepsilon(t))} + jM\left[\frac{d(\alpha(t)-\varepsilon(t))}{dt}\right]i_S(t)e^{j(\alpha(t)-\varepsilon(t)}$$

5.2.1.1 The Torque Equation

A force *f* is produced when a conductor of length *l and carrying a current i* is placed in a magnetic field with a flux density B*:*

F=Bil

In an induction motor a torque is produced when the rotor current flows through the rotor conductors that lie in the magnetic field produced by the stator current (mmf). Rotor current does not contribute to rotor torque as its maximum value lies where current density is zero [17].

The stator mmf seen by the rotor windings is found by multiplying that seen by the stator by $e^{-j\varepsilon(t)}$. *See figure 14.*

$$\vec{F}_S^{\,r}(t) = \vec{F}_S^{\,s}(t)e^{-j\varepsilon(t)} \text{.....(21)}$$

When leakage is included, then the mm is reduced by a factor of ℵ. Assuming that iron has zero reluctance, the mmf is dropped across the two air gaps and the flux density space vector **produced by the stator but seen by the rotor** is:

$$\vec{B}_{S_R}(t) = \frac{\mu_0}{2h}\aleph \vec{F}_S^{\,r}(t)$$

$$= \frac{\mu_0 \aleph N_S}{2h}\vec{i}_S^{\,r}(t) \text{.....(22)}$$

This flux density space vector is aligned with the stator current space vector as seen by the stator windings.

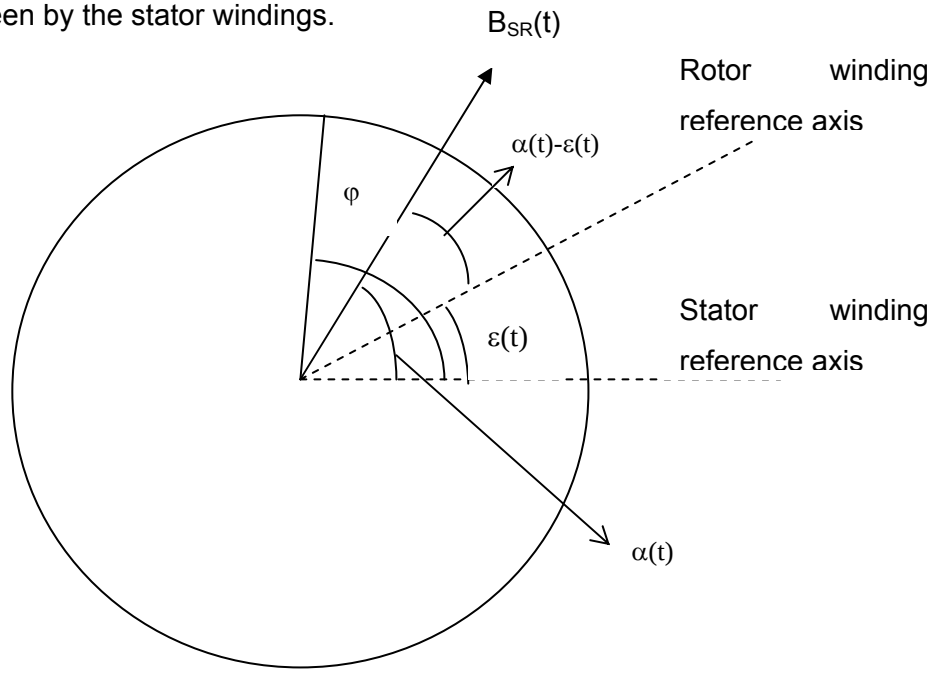

Figure 15: Stator mmf seen by rotor [17]

Assuming a sinusoidal flux distribution around the rotor circumference, the magnitude of at angle φ is.

$$\frac{\mu_0}{2h} i_S(t) \cos\left[\varphi - \left[\alpha(t) - \varepsilon(t)\right]\right]$$

The effective rotor current at angle φ is needed to calculate the torque produced.

The rotor current profile around the rotor is approximated by an effective **rotor surface current density**, which can be shown to be [16]:

$$J_R(\varphi, t) = -\frac{N_R}{2r} i_R(t) \sin\left[\varphi - \beta(t)\right] \text{.....(23)}$$

Then the torque contributed by an **elemental conductor** at angle φ to the **rotor winding reference axis** with width **rdφ** is:

dT_e = -r x **flux density** x **rdφ** x **surface current density** x **axial length**

$$= -r \frac{\mu_0 \aleph N_S}{2h} i_S(t) \cos\left[\varphi - \left[\alpha(t) - \varepsilon(t)\right]\right] r d\varphi \left[-\frac{N_R}{2r} i_R(t) \sin\left[\varphi - \beta(t)\right] \right] l$$

$$= \frac{\mu_0 r l \aleph N_S N_R}{4h} i_S(t) i_R(t) \cos\left[\varphi - \left[\alpha(t) - \varepsilon(t)\right]\right] \sin\left[\varphi - \beta(t)\right] d\varphi$$

but $M = \frac{3\mu_0 r l N_S N_R \pi}{8h}$

Therefore:

$$dT_e = \frac{2}{3\pi} M i_S(t) i_R(t) \cos\left[\varphi - \left[\alpha(t) - \varepsilon(t)\right]\right] \sin\left[\varphi - \beta(t)\right] d\varphi \text{.....(24)}$$

The **total electromagnetic torque** is obtained by integrating around the rotor circumference:

$$T_e = \frac{2}{3\pi} M i_S(t) i_R(t) \int_0^{2\pi} \cos[\varphi - [\alpha(t) - \varepsilon(t)]] \sin[\varphi - \beta(t)] d\varphi$$

and **cos(a)sin(b)=1/2[sin(a+b)+sin(b-a)**

therefore:

$$T_e = \frac{1}{3\pi} M i_S(t) i_R(t) \int_0^{2\pi} [\sin[2\varphi - \alpha(t) - \beta(t) + \varepsilon(t)] + \sin[[\alpha(t) - \varepsilon(t)] - \beta(t)]] d\varphi$$

$$= \frac{2}{3} M i_S(t) i_R(t) \sin[[\alpha(t) - \varepsilon(t)] - \beta(t)] \text{.....(25)}$$

The angle $[\alpha(t)-\varepsilon(t)]-\beta(t)$ is the angle between the stator current space vector and the rotor current space vector. The sine term indicate that the component of the stator current space vector that is **quadrature** to the rotor current space vector is the significant component.

Therefore:

$$T_e(t) = \frac{2}{3} M i_{sq}(t) i_R(t) \text{.....(26)}$$

Where $I_{sq}(t) = \sin[[\alpha(t)-\varepsilon]-\beta(t)]$ is the component of the stator current space vector producing the flux **quadrature** to the rotor current (mmf) space vector.

The quadrature component of the stator current space vector produces the field maximum in the position where rotor current density is at a maximum, thus producing the torque [17]. The direct component of the stator current space vector produces the field when rotor current density is zero and therefore makes no contribution to the electromagnetic torque produced.

AC motors (both synchronous and induction) can therefore be described by the following four space vector equations:

$$\vec{v}_S^{\,s}(t) = R_S \vec{i}_S^{\,s}(t) + L_S \vec{i}_S^{\,s}(t) + M \frac{d}{dt}\left[\vec{i}_R^{\,r}(t) e^{j\varepsilon(t)}\right] \quad \text{.....(27)}$$

$$\vec{v}_R^{\,r}(t) = R_R \vec{i}_R^{\,r}(t) + L_R \frac{d}{dt}\vec{i}_R^{\,r}(t) + M \frac{d}{dt}\left[\vec{i}_S^{\,s}(t) e^{-j\varepsilon(t)}\right] \quad \text{.....(28)}$$

$$\frac{d\varepsilon(t)}{dt} = \omega(t) \quad \text{.....(29)}$$

$$J \frac{d\omega(t)}{dt} = \frac{2}{3} M i_S(t) i_R(t) \sin\left[\left[\alpha(t) - \varepsilon(t)\right] - \beta(t)\right] - T_L(t) - T_F(t) \quad \text{.....(30)}$$

Where $\omega(t)$ is the angular velocity of the rotor

$T_L(t)$ is the opposing load torque

$T_F(t)$ is the opposing friction torque

6. FIELD ORIENTED CONTROL OF INDUCTION MOTORS

The **rotor flux density** space vector can be calculated from [17]:

$$\vec{B}_R^r(t) = \frac{\mu_0}{2h}\left[\vec{F}_R^{\,r}(t) + \aleph \vec{F}_S^{\,r}(t)\right]$$

$$= \frac{\mu_0}{2h}\left[N_R \vec{i}_R^{\,r}(t) + \aleph N_S \vec{i}_S^{\,s}(t) e^{j\varepsilon(t)}\right]$$

then substituting $L_R = \frac{3\mu_0 rlN_R^2\pi}{8h} = \frac{\mu_0 N_R}{2h}\left[\frac{3rlN_R\pi}{4}\right]$

and $M = \frac{3\mu_0 rlN_S N_R\pi}{8h} = \frac{\mu_0 \aleph N_S}{2h}\left[\frac{3rlN_R\pi}{4}\right]$

therefore $\vec{B}_R^r(t) = \frac{4}{3rlN_R\pi}\left[L_R \vec{i}_R^{\,r}(t) + M\vec{i}_S^{\,s}(t)e^{-j\varepsilon(t)}\right]$.....(31)

The stator and rotor **self-inductances** can be expressed in terms of **mutual and leakage inductances**:

$$L_S = M + \sigma_S M = [1+\sigma_S]M \text{.....}(32)$$

$$L_R = M + \sigma_R M = [1+\sigma_R]M \text{.....}(33)$$

where σ_S and σ_R are defined as the stator and rotor leakage coefficients respectively. Substituting equation 32 into equation 31:

$$\vec{B}_R^r(t) = \frac{4M}{3rlN_R\pi}\left[[1+\sigma_R]\vec{i}_R^{\,r}(t) + \vec{i}_S^{\,S}(t)e^{-j\varepsilon(t)}\right]\text{.....}(34)$$

It is important to note that current space vector inside the brackets determines the rotor flux density space vector. This is defined as the **magnetising current space vector**. Referenced from the stator winding reference axis:

$$\vec{i}_{m_R}^{\,s}(t) = [1+\sigma_R]\vec{i}_R^{\,r}(t)e^{j\varepsilon(t)} + \vec{i}_S^{\,s}(t)$$

$$= i_{m_R}(t)e^{j\rho(t)} .....(35)$$

where $\rho(t)$ is the angle of the magnetising current referenced to the stator winding reference axis.

Vector control deals with the control of the magnitude of the rotor magnetising current and the control of torque via the quadrature component of the stator current space vector. Analysis will be done by referencing to the **magnetising current reference axis** that will be denoted by the superscript 'm'.

The stator current space vector then becomes:

$$\vec{i}_S^{\,m}(t) = \vec{i}_S^{\,s}(t)e^{-j\rho(t)}$$

This vector is then resolved into direct and quadrature components:

$$\vec{i}_S^{\,m}(t) = i_{sd}(t) + ji_{sq}(t).....(36)$$

where $i_{sd}(t)$ is the direct component (aligned with the rotor flux axis)

$i_{sd}(t)$ is the quadrature component (perpendicular to the rotor flux axis)

The stator current space vector diagram then becomes [16, 17]:

$i_{sq}(t)$

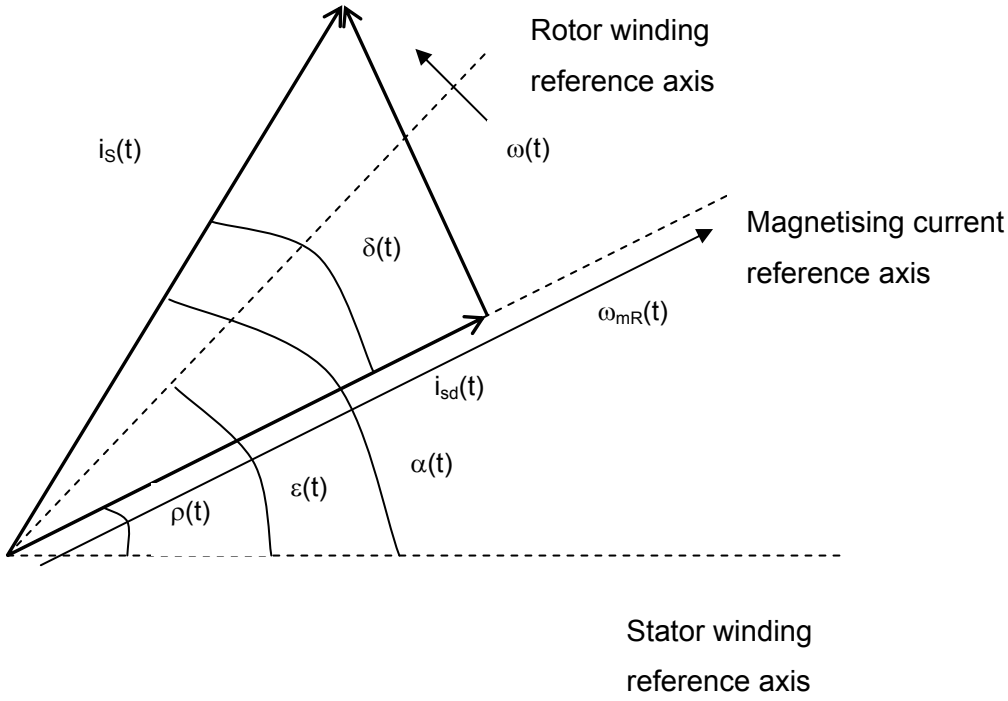

Figure 16: Stator current space vector diagram

Where $\omega_{mR}(t)$ is the angular velocity of the magnetising current flux axis relative to stator winding reference axis.

From equation 25: $T_e = \frac{2}{3} M i_S(t) i_R(t) \sin\left[\left[\alpha(t) - \varepsilon(t)\right] - \beta(t)\right]$

It can be shown that the torque equation for induction motors is given by the following equation:

$$T_e = \frac{2}{3} \frac{M}{1+\sigma_R} i_{m_R}(t) i_{sq}(t) \text{.....(37)}$$

I_{mR} by definition controls rotor flux magnitude, it is necessary to determine how it can be controlled via the stator current i_S. The relationship between $I_{mR}(t)$ and $I_{sd}(t)$ and $I_{sq}(t)$ is as follows:

$$\frac{L_R}{R_R}\frac{d}{dt}\left[i_{m_R}(t)\right]+i_{m_R}(t)=i_{sd}(t)$$

$$=\tau_R\frac{d}{dt}\left[i_{m_R}(t)\right]+i_{m_R}(t)=i_{sd}(t).....(38)$$

and

$$\tau_R\left[\omega_{m_R}(t)-\omega(t)\right]i_{m_R}(t)=i_{sq}(t).....(39)$$

Combined with:

$$J\frac{d\omega(t)}{dt}=\frac{2}{3}\frac{M}{1+\sigma_R}i_{m_R}(t)i_{sq}(t)-T_L(t)-T_F(t).....(40)$$

$$\frac{d\varepsilon(t)}{dt}=\omega(t).....(29)$$

describes the behaviour of an induction motor under field-orientated control.

6.1 Control Strategy for Field-Oriented Control

The stator current components $i_{sd}(t)$ and $I_{sq}(t)$ are transformed to the stator currents $i_{S1}(t)$, $i_{S2}(t)$ and $i_{S3}(t)$ via two intermediate currents which are the direct and quadrature components referenced to the stator winding reference axis as opposed to the magnetising current axis.

The stator current space vector referenced from the stator winding reference axis is:

$$\vec{i}_S^{\,s}(t) = i_{S1}(t) + i_{S2}(t)e^{j\frac{2\pi}{3}} + i_{S3}(t)e^{j\frac{4\pi}{3}}$$
$$= i_{sa}(t) + ji_{sb}(t) \ldots\ldots\ldots\ldots\ldots\ldots\ldots (41)$$

Referencing the stator current to the magnetising current reference axis:

$$\vec{i}_S^{\,m}(t) = i_{sd}(t) + ji_{sq}(t) = \vec{i}_S^{\,s}(t)e^{-j\rho(t)}$$
$$= \left[i_{sa}(t) + i_{sb}(t)\right]e^{-j\rho(t)} \ldots\ldots\ldots\ldots\ldots\ldots\ldots (42)$$

Therefore:

$$i_{sd}(t) = i_{sa}(t)\cos\rho(t) + i_{sb}(t)\sin\rho(t) \ldots\ldots\ldots (43)$$
$$i_{sq}(t) = i_{sb}(t)\cos\rho(t) - i_{sa}(t)\sin\rho(t) \ldots\ldots\ldots (44)$$

Then knowing the following:

$$i_{sa}(t) = i_{S1}(t) + i_{S2}(t)\cos\frac{2\pi}{3} + i_{S3}(t)\cos\frac{4\pi}{3} \ldots\ldots\ldots (45)$$

$$i_{sb}(t) = i_{S2}(t)\sin\frac{2\pi}{3} + i_{S3}(t)\sin\frac{2\pi}{3} \ldots\ldots\ldots\ldots\ldots\ldots (46)$$

and assuming an isolated neutral, therefore:

$$i_{S1}(t) + i_{S2}(t) + i_{S3}(t) = 0 \ldots\ldots\ldots .(4)$$

The following relationships relating $i_{sb}(t)$ and $i_{sa}(t)$ to the stator currents can be derived:

$$i_{S1}(t) = \frac{2}{3} i_{sa}(t) \text{.....(48)}$$

$$i_{S2}(t) = \frac{1}{\sqrt{3}} i_{sb}(t) - \frac{1}{3} i_{sa(t)} \text{.....(49)}$$

$$i_{S3}(t) = -\frac{1}{3} i_{sa}(t) - \frac{1}{\sqrt{3}} i_{sb}(t) \text{.....(50)}$$

These equations lead to the following block diagram for field-oriented control:

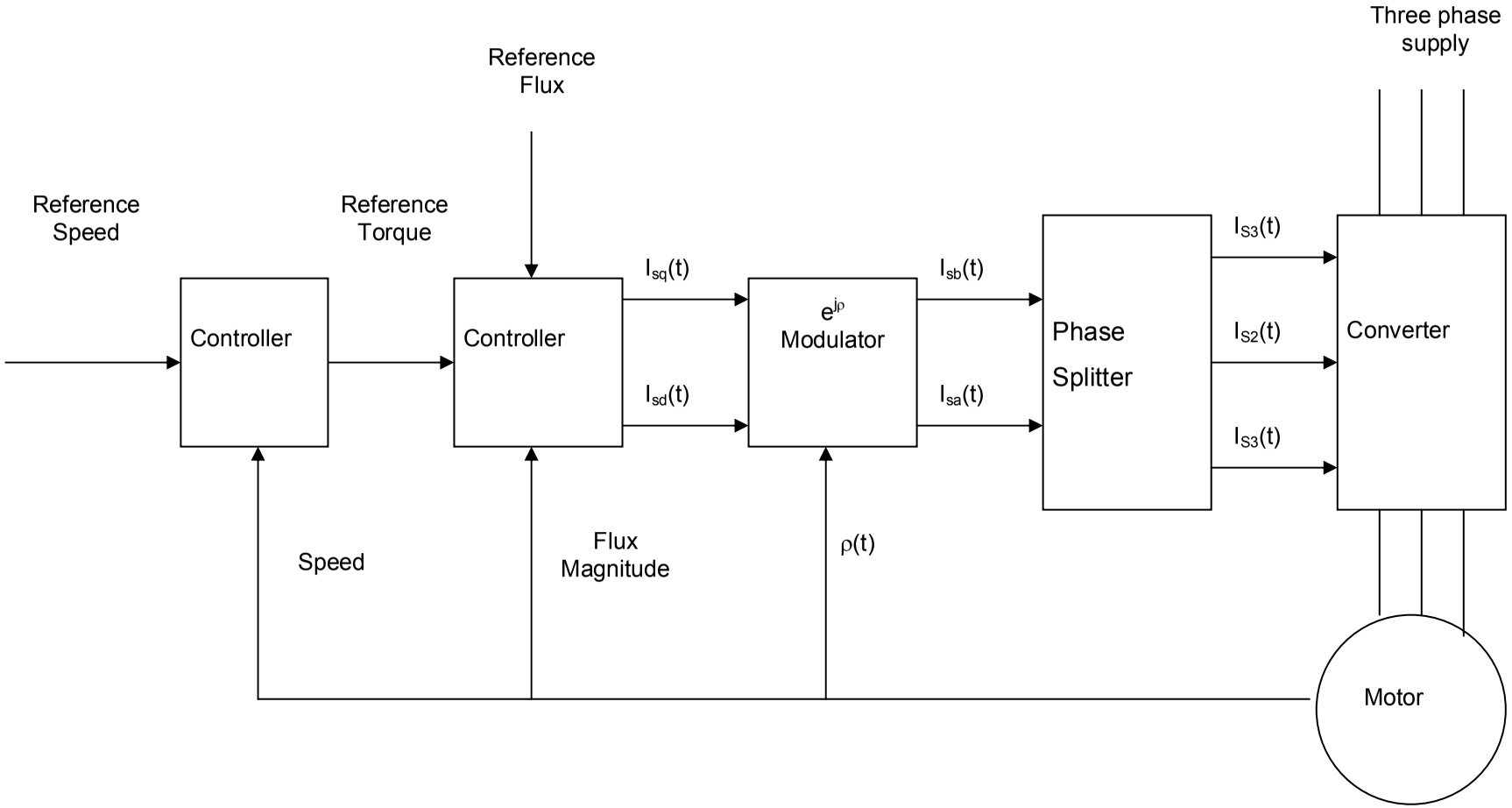

Figure 17: Block diagram of field oriented control of an induction motor

7. IMPLEMENTATION STRATEGY

The theory presented in the previous chapter illustrates that an induction motor under field-oriented control can be manipulated to deliver accurate torque control. This makes it an ideal control philosophy for the use in a programmable load.

Implementation of a programmable load utilising an induction motor to generate the simulated load torque would involve driving the motor in opposition the motor under test (MUT).

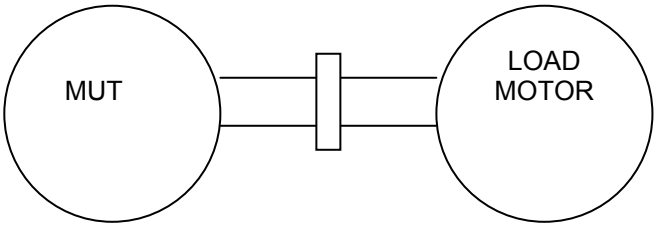

Figure 18: Rotor shafts coupled

Figure 18 illustrates the method of applying an opposing torque by coupling the rotor shafts of the MUT and the load motor.

7.1 Control of Load Motor

The theory of field-oriented (vector) control illustrates that it is a viable solution to provide the accurate control required to simulate industrial load conditions. Vector control provides good dynamic response at the expense of a complex converter. The development of such a converter would, in the opinion of the author, be a time-consuming and complex task. This would lead to high costs in terms of man hours required for the development.

An alternative to developing a converter with vector control functionality is to purchase a unit with the required functionality off the shelf. This is viable as many modern converters utilise vector control due to its inherent advantages.

An AC motor is chosen above the alternative of a DC motor (which is highly controllable) as induction motors are widely utilised, inexpensive, readily available and easily repairable. Four quadrant variable speed drives are used in electrical braking applications including elevators, winches and cranes [18]. This application is a variation on this type of braking application.

The proposed schematic of the programmable load utilising an off-the-shelf VSD to implement field-oriented control is illustrated in figure 19:

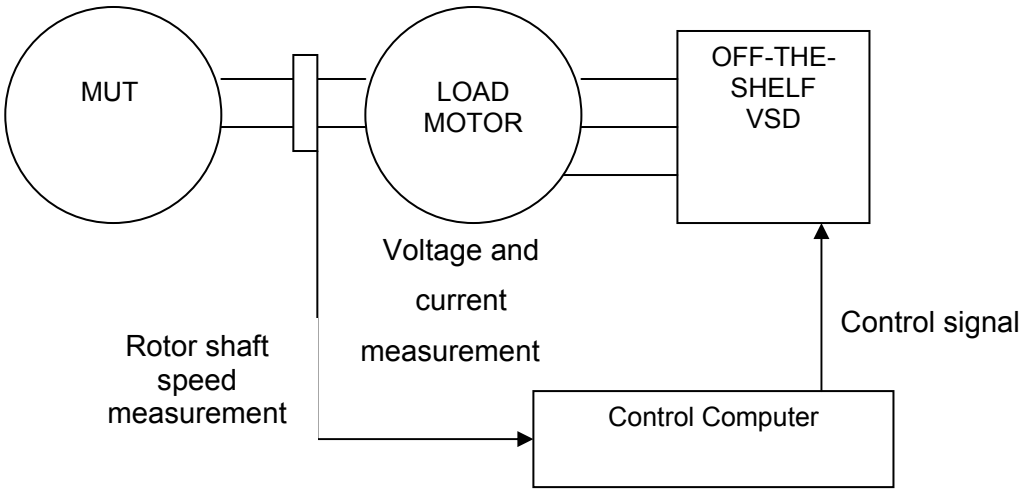

Figure 19: Block diagram of Programmable Load

Figure 19 shows that a control computer will be utilised to control the output torque via the VSD. The aim of the system is to simulate the torque characteristics of industrial loads as described in previous chapters. The characterisation of loads as torque vs. speed functions means that the control system is inherently dependent on shaft speed to determine the required torque. This leads to a feedback system that has the rotational speed of the rotor shaft as its primary variable. This system is of the form represented in figure 17 but utilises a variable speed drive to eliminate the need to develop software to compensate for the required phase-splitting and angular rotations.

7.2 Control Software

The control software is required to measure the angular velocity, calculate the appropriate torque value for that specific velocity and output a signal controlling the output torque of the variable speed drive. Under steady state conditions the torque output will follow a specified torque vs. speed curve. Dynamic conditions are more complex in that inertia has to be accounted for. Measurement of angular acceleration becomes crucial as the product of inertia and angular acceleration determines the torque generated by the load under these conditions (see previous chapter).

7.3 Key Issues Affecting Performance

Parameters that determine the performance of the programmable load are:

- **Accuracy of torque** – Modern VSD's are accurate to within a few percent; measurements will need to be taken to determine whether the system is accurately simulating the required torque values for set points.
- **Response Time** – To simulate loads the response of the load will have to be very fast to eliminate a significant time lag which will cause the accuracy of the system to be poor.
- **Low Speed Performance** – Both constant torque and constant power loads have their maximum torque requirement at speeds approaching zero revolutions per minute. Ensuring that this torque is accurate is important as many drives lose accuracy at such low speeds.

8 EQUIPMENT AND SOFTWARE

8.1 Equipment

The following equipment is required to implement the programmable load:

- Control PC
- Variable Speed Drive
- Induction Motor
- Tachometer
- Analogue-to-Digital (A/D) Converter
- Digital-to-Analogue (D/A) Converter

8.1.1 VARIABLE SPEED DRIVE

Vector torque control drive
0-10V analogue torque control input
4-20mA torque measurement output preferably

Several VSD's were considered for the implementation. The SAFTRONICS VFX40-146 vector torque drive was chosen as a suitable drive for the following reasons.

- Vector control functionality
- Widely used in South Africa
- Manufacturer provides good back-up to users of the drive
- Large amount of material available on drive capabilities
- Flexibility- Utilises Input/Output (I/O) cards for specific interface and controls
- Choice of I/O cards available
- Zero Speed command
- Manual Torque Control with proper I/O card installed

The availability of a range of I/O cards to personalise the drive to a specific function was an important factor in the choice of VSD. The

utilisation of a variable speed drive for a programmable load implementation is a one-off installation that could produce certain complications not necessarily found under normal operating conditions for drives in industry. This potential means that a certain amount of flexibility may be required to adjust to these unique circumstances. The I/O card allows the user to specify which variables are to be manually monitored and also provides control over the certain areas of operation of the VSD e.g. vector control.

The cards chosen for the load implementation are:

- **AIO Analogue I/O card-**Enables analogue inputs of frequency, setting, torque limit values etc.

8.1.2 Induction Motor

Maximum power = 75kW. The power rating of the motor was adjusted from the initial value of 150 kW to 75 kW due to the limitations of the programmable supply. The programmable supply is limited to 80kVA. Rating the load any higher than this would mean it is capable of operating in a range into which the equipment under test (EUT) cannot be operated due to the inherent limitations of the supply.

8.1.3 Analogue Interface

The analogue interface cards were specified according to the following criteria:

- Resolution
- Number of interface channels required
- Software drivers available
- Sampling frequency

8.1.3.1 Resolution

All converters are required to be minimum 12-bit converters.

8.1.3.2 Number of Channels Required

The following inputs are required as a minimum:

- Actual angular velocity
- Actual angular acceleration
- Angular position of shaft (optional)

8.1.3.3 Software Drivers available

To use the analogue interface cards effectively without understanding the low-level design of the card, software drivers are required. These software drivers are accessed from the program and perform card configuration, analogue input and output, timing and other functions. The availability of high-level drivers makes it possible to utilise card effectively in a much shorter time than if the card were to be accessed directly.

8.1.3.4 Sampling Frequency

The A/D card will be measuring both torque and angular velocity transients. Experience with operating the current programmable supply has shown that a sampling frequency of 4 kHz is sufficient for control purposes. Modern A/D cards are capable of sampling at frequencies in excess of 100kHz.

8.1.3.5 Analogue interface card

It is preferable to utilise a card that incorporates both A/D and D/A functionality on a single board. This means that a driver is only required for a single card, simplifying the process. During the program development a single card can be addressed to both input and output signals and data. The card chosen was the Eagle Technology **PCI-30 GA**. This card incorporates 16 A/D input channels and 4 D/A output channels which are more than adequate for the required application. Eagle Technology also has driver software available that will interface

with most windows based programming languages. A wide range of user information and assistance is available from their website and from the company itself as it is a local company.

8.2 Software

8.2.1 Programming Language

A Windows based program needs to be developed. Visual Basic is often used to create applications due to the ease of creating Windows layouts in it. Visual Basic creates code that is interpreted as it is run and this result in slower applications. C++ executes code directly, which means faster applications. C++ is also capable of both high level and low-level interfacing. C++ will be utilised for development of the control program for the programmable load.

8.2.2 Software Outline

The software to be produced must perform the following functions:

- Use the shaft velocity (or other signals) to calculate the desired output torque value to the field-oriented drive
- Output torque feedback is required to verify the accuracy of the torque calculation

The output torque will be calculated according to the dynamic torque characteristic equation illustrated in chapter 3. This model requires two states to be considered: steady state and dynamic.

The **steady state** component requires the following parameters for complete description:

- Load type
- Initial torque
- Maximum torque
- Load co-efficient (for variable torque load)
- Power (for constant power load)

- Rotational shaft velocity (input from analogue-to-digital interface)

The **dynamic** component requires:

- Moment of inertia specific to particular load
- Rotational acceleration (input from analogue-to-digital interface)

These variables cover the model parameters required by the software for load simulation purposes.

The user interface to set up the load is also important. The following functionality is required:

- Non real-time input of parameters
- Save and recall of specific load cases

The following data is required to be stored and plotted on graphs for easy analysis:

- Actual angular velocity vs. time
- Actual angular acceleration vs. time
- Torque vs. time

8.3 Control Algorithm

Following the implementation strategy discussed previously, the flow chart for the control algorithm is as follows:

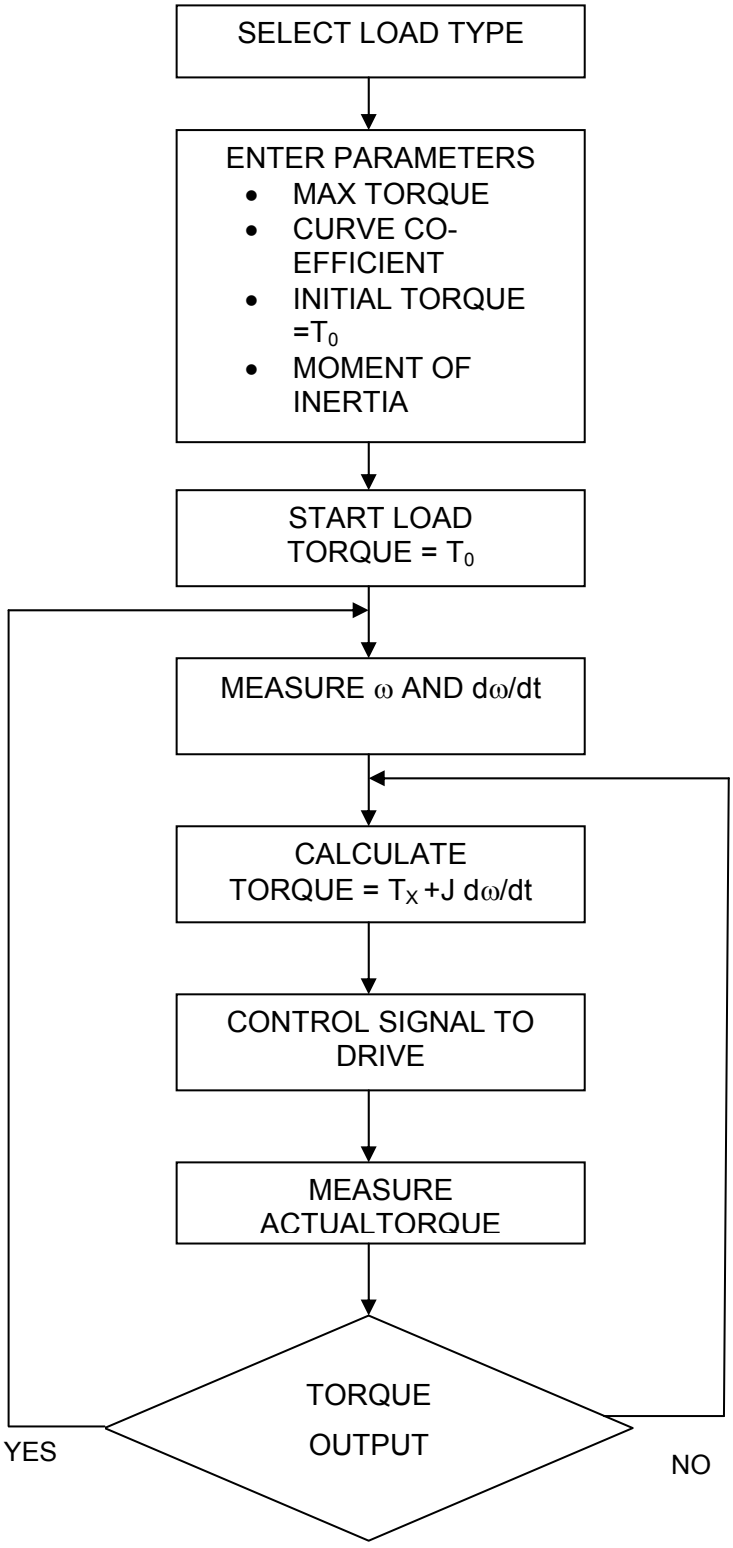

Figure 20: Control flow structure

8.3.1 Process Flow

The program structure will start off with setting of load type i.e. quadratic, constant power or constant torque. It will then flow into specifying the load parameters for any specific individual load and also the initial torque for any set load. The starting of the load will be synchronised with that of the programmable supply for ease of use and consistent measurements plotted against time. After the start-up rotational velocity will be measured and this will be the control variable for accurate control of the load output torque. The constant T_x as described in the control algorithm is the desired torque according to a specific torque-speed characteristic. Feedback of output torque will be required to ensure accuracy of the system.

9. HARDWARE CONSTRUCTION

9.1 Power Supply

The power supply to the programmable load is a 3-phase supply via the 100kVA G.E.C transformer in the Wits machines laboratory.

9.2 Data Acquisition Card

The data acquisition card for the implementation of the programmable load was changed during the course of work from the originally specified Eagle PCI30GA card to the Eagle PCI730. The reason for the change in the card was due to the inability of the PCI30GA card to adjust the number of data units transferred at a time from the card memory buffer to the computer memory buffer. This inflexibility led to a control loop that could only respond to a maximum of less than 100 times a second at a high sampling frequency of 100 kHz.

9.3 Variable Speed Drive

The variable speed drive utilised is the Emotron VFX40-146. This drive was utilised due to the fact that Saftronics South Africa supplied the drive at cost price that resulted in a major cost saving. The change in

variable speed drive was accepted once it had been verified that the VSD had the necessary control capabilities and external inputs with which the control of the drive could be implemented.

9.4 Motor and Drive Connections

The Emotron VectorFlux VFX40-146 variable speed drive has a terminal strip inside the drive panel itself that allows interfacing with external control and/or measurement equipment. The VectorFlux drive was initially connected according to the instructions provided in the instruction manual. Figure 21 is an indication of the basic wiring layout for the VFX40-146 drive.

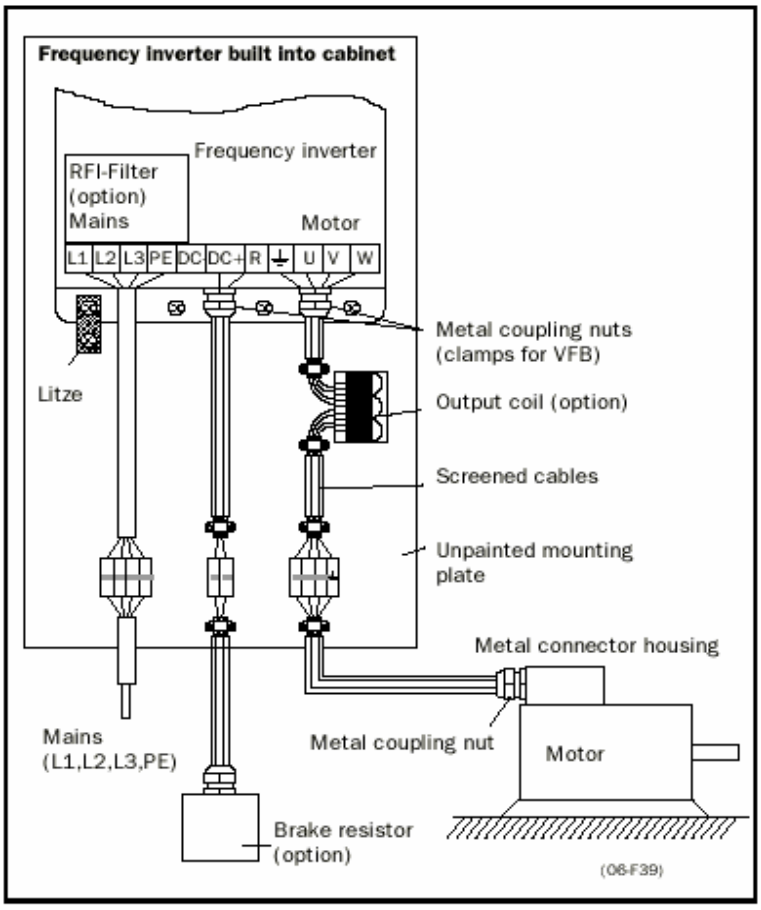

Figure 21: Basic wiring for Vectorflux drive [18]

Connections L1, L2, L3 and PE as shown in the graphic were connected to the required 380V 3-phase supply in the laboratory. The motor was connected in delta without the optional output coil and brake

resistor. The cabling utilised for the drive and motor supply were both sized to handle the 146A maximum current of the variable speed drive.

Figure 22 shows the Vectorflux VFX drive on the left and the wiring to the drive on the right. The image shows the connections to the power supply and the cabling out to the induction motor.

Figure 22: Drive and wiring connections

Once the basic construction of the VSD had taken place it was possible to start the process of operating the VSD and determining the required internal settings of the VSD for independent operation, operation under analogue control and operation via analogue inputs from an independent controller.

9.5 Basic System

Operation of the Vectorflux drive is possible through the control panel on the front of the drive. Connections on the terminal strip on the inside of the drive are also required depending on the mode of operation required. The control board connector has the following connections that are relevant to the operation of the drive in this particular application:

- 2 Analogue inputs.
- 2 Analogue outputs.
- 2 Digital inputs.

- 2 Digital outputs.
- ±10Volt DC supply.
- +24 Volt DC supply.
- Run right and Run left only option.

The importance of these settings in the operation of the drive in this application will be discussed later in the report. The minimum wiring to start the drive and implement a basic form of external control is shown in figures 23 and 24.

Figure 23 shows the minimum control wiring required for starting up the drive.

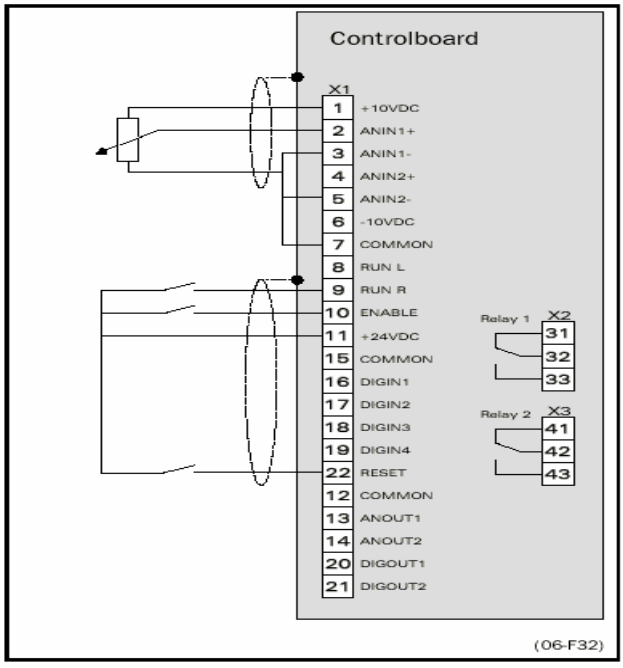

Figure 23: Minimum control wiring [18]

The basic connections for manual uni-directional operation according to figure 3 are as follows:

- 10: HIGH – This is implemented by connecting terminal 10 to terminal 11(+24 VDC supply)

- Basic external analogue control is achieved by utilising the ±10Volt DC supply and connecting a potentiometer across the supply (connections 1 and 6).

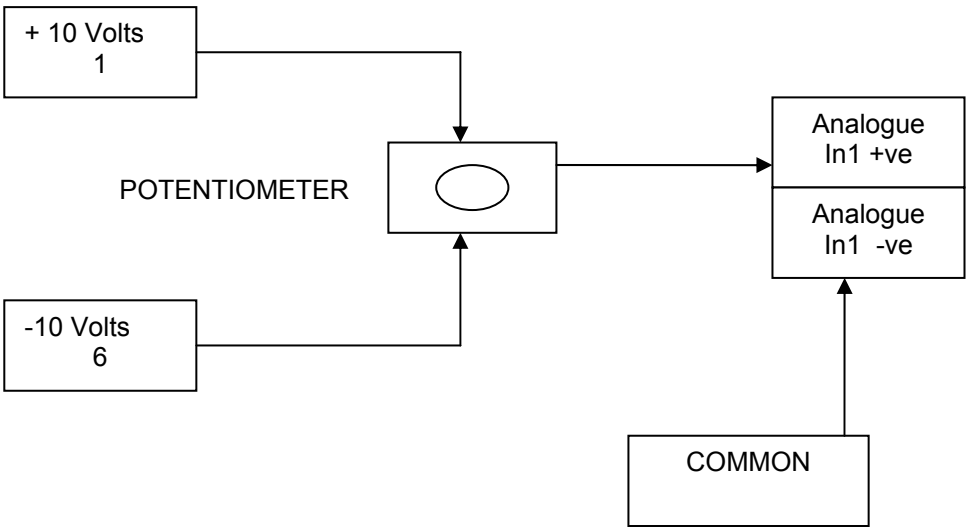

Figure 24: Wiring for manual uni-directional analogue control

The main purpose of running the drive with the 10kΩ potentiometer was to enable the familiarisation and testing of the drive. In this manner the limits and responses of the drive could be tested. This set-up allowed rotation in one direction and allowed speed or torque control in that direction. Furthermore, this allowed for the setting up of the drive for interfacing with the control computer. The VFX40-146 VSD has a complex menu system and a host of functions that can be set for operation in a wide variety of applications. These settings need to be checked to ensure the drive operates as required for a specific application. This is especially true for operation under experimental conditions. Using the potentiometer for manual control meant that most of the variable speed drive settings could be tested and adjusted as required prior to the introduction of the digital data acquisition and control system. This method eliminated an element of risk from the development process.

10. SYSTEM CONTROL IMPLEMENTATION

The control implementation has 2 major components that affect:

- Setting up of the VSD to enable control via an external source (this refers to control panel settings as well as wiring connections).
- The external digital control system via data acquisition hardware and control software.

10.1 Variable speed drive settings

The following drive parameters are set up in a manner that ensures easy interaction with external control sources:

- Drive Mode.
- Analogue inputs.
- Rotation and Speed direction.
- Analogue outputs.
- Run-Stop Control.
- Programmable Load Operating Connections.

10.1.1 Drive Mode

The drive mode has three possible settings that relate to the internal control loops of the VSD. These are:

- Speed.
- Torque.
- V/Hz.

The drive mode determines the parameter that control loops will track i.e. speed or torque. The V/Hz parameter follows a loop that controls frequency and allows multi-motor operations from the VSD. This specific application requires control of the output torque and consequently the drive mode selected is torque.

10.1.2 Analogue Inputs

The analogue inputs are only available for the user when the VSD's internal PID controller is de-activated. Once the PID controller is

activated all value are derived from this controller and its set-point values. The analogue input variable can than be set to either control torque or speed. Figure 25 shows the menu choices and their functions as displayed in the control panel of the VSD. The reference value referred to in the diagram is the input voltage.

411 AnIn 1 Funct Stp **Speed**	
Default:	Speed
Selection:	Off, Speed, Torque
Off	Input is not active
Speed	Reference value is set for Speed Control
Torque	Reference value is set for Torque Control

Figure 25: Analogue input settings [18]

The drive mode and analogue input need to be co-ordinated for control of a particular parameter. In this application we desire torque control, therefore the drive mode selected is torque and similarly the variable that we input is torque.

Figure 26 shows the block diagram for the internal control process of the VSD. It clearly indicates the need to de-activate the PID process and the differentiation between operation in speed mode and torque mode. In the torque mode of operation, the output torque of the drive tracks the input voltage received at the analogue input.

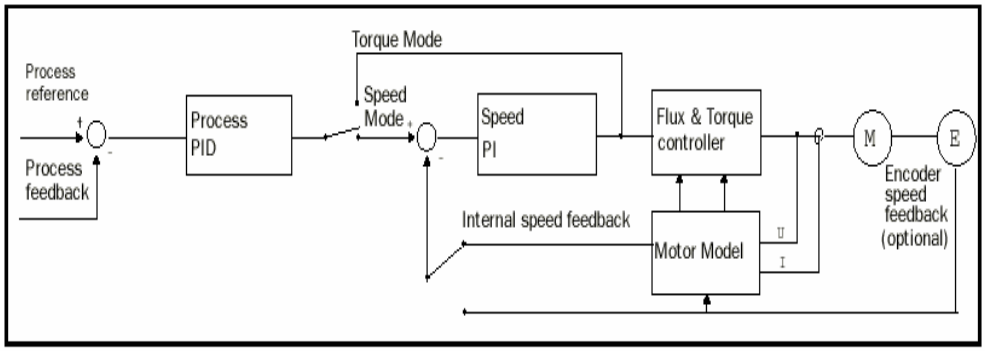

Figure 26: Internal closed loop control of VSD [18]

10.1.3 Analogue Input Polarity

The setting of polarity of the analogue inputs is one of several settings that need to be properly set to allow rotation in both directions i.e. clockwise and anti-clockwise. With a bipolar setting of the input variable the drive will recognise a reference signal from –10V to +10V, whereas with a uni-polar input only the positive signals are recognised. This has implications for changing the direction of rotation of the drive during operation. The drive has been set up for operation in uni-polar mode. Compatibility problems were experienced with the D/A card when operating in bipolar mode.

10.1.4 Rotation and Speed Direction

The drive allows rotation in two directions. Setting rotation in both directions enables bipolar analogue inputs. Setting of the speed direction enables the start signals to be read in both directions and the voltage polarity to determine the direction of rotation. If this is not set to recognise both directions any start signal from the control panel will be recognised as a signal to rotate in one direction. The analogue input will be read as an absolute value that determines magnitude, which in this case would be the amount of torque required. This setting has been revised to allow operation in one direction only. This is acceptable for this application as the drive will be acting as an opposing torque (or effectively a type of brake).

10.1.5 Run-Stop Control

The run-stop control can be received from a number of sources either internal to the drive or from external signals. The default setting is to receive the command from the start and stop buttons on the control panel of the drive. For this application a start stop signal from the control computer would allow full control of the drive and hence the programmable load from the control computer. This is achieved by

setting the source of the run-stop control to REMOTE, which then sources the run-stop commands from the terminal strip on the drive. Pins 8 and 9 on the strip are the Run Left and Run Right commands respectively. A +24 Volt signal on either of these will turn the motor in that particular direction.

10.1.6 Programmable Load Operating Connections

Manual control of the drive first had to be established prior to computerising the control. This was done by providing the proper connections to the drive as discussed above and manually controlling the input signal and the run-stop control as described in table 3.

PIN	DESCRIPTION	NOTE
2	Analogue Input +ve	Torque control signal
3	Analogue Input -ve	Signal common
7	Neutral/Common	
8	Run Left	Enables rotation to Left
9	Run Right	Enables rotation to Right
10	Enable	Enables drive operation
11	+24 Volt	High signal for 8, 9, 10
12	Neutral/Common	Neutral reference for 13
13	Analogue Output 1	Output Speed

Table 3: Control connections

Figure 27 illustrates the connections made to implement analogue control of the VSD via a data acquisition card. It should be noted that the analogue outputs from the VSD were replaced by a more reliable method of using a filtered tachometer signal for speed measurement.

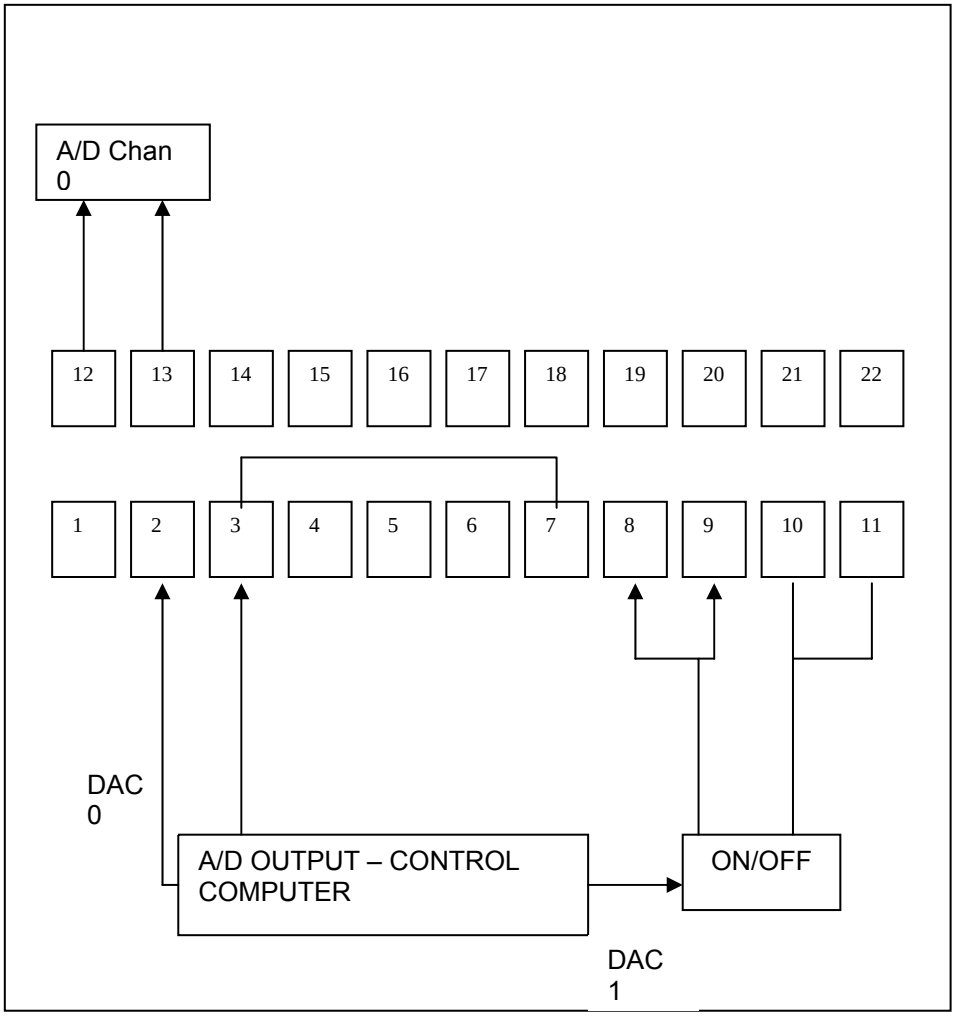

Figure 27: Control connections to VSD terminal strip

Terminal 10 enables the operation of the drive and allows the rotation of the motor. Terminals 8 and 9 are Run Left and Run Right respectively. With both of these enabled the direction of rotation as well as the amount of torque is determined by the magnitude and polarity of the signal received at Analogue Input 1. Note that the Neutral of the D/A card and the VSD are joined to provide a common reference for the polarity. The control program determines the output torque from the signal received from analogue output 1 (programmed to output the rotational speed of the motor) of the VSD. This torque is then outputted as a 0-10 V signal to the VSD.

10.2 Input Circuit and Filtering

The system utilises motor speed as the control variable for the process. A digital tachometer is used to measure motor speed. The tachometer has an output equal to 90 Volts/1000 r.p.m. This is scaled to a ratio of 10 Volts/1475 r.p.m by a resistive divider. The signal is then input through a differential amplifier and filtered to eliminate random noise with a second order Butterworth filter with a cut-off frequency that is between 100 and 110 Hz (actual frequency 106.7 Hz). The input circuit and filter are shown in figure 28.

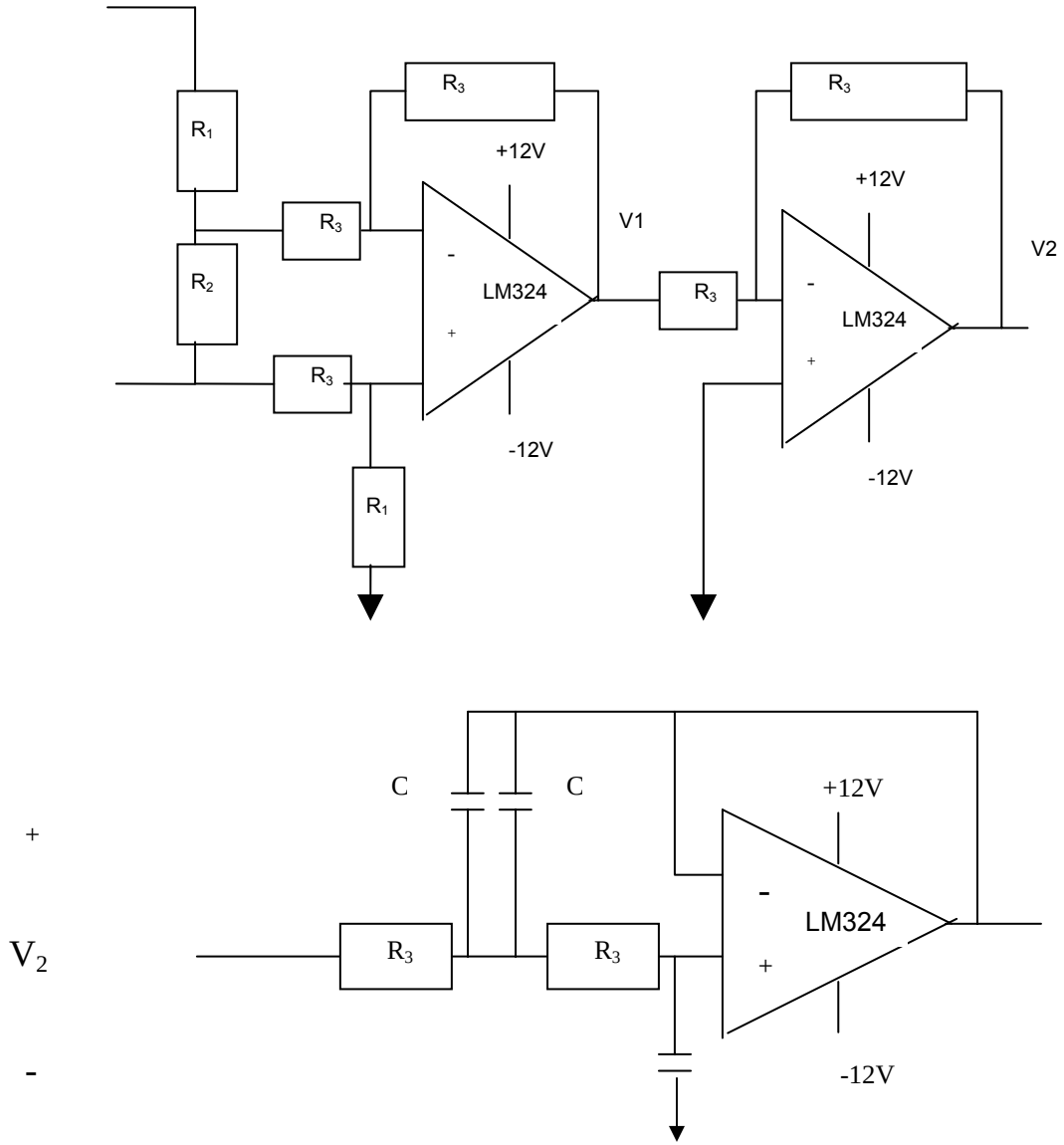

Figure 28: Resistive divider, differential amplifier and Butterworth filter

The cut-off frequency of the Butterworth filter is:

$$F_c = 1/(2.83 \times \pi \times R_3 \times C)$$

The component values are listed in table 4.

COMPONENT	VALUE
R_1	8.9kΩ
R_2	1kΩ
R_3	27kΩ
C	39Nf
Operational amplifier	LM324

Table 4: Component values

10.3 Software Implementation

The data acquisition card that was chosen for the final implementation was the Eagle Technology PCI 730 card.

The basic process for the implementation of this control process consists of three parts:

- Measurement of control variable – i.e. ω.
- Calculation of desired value.
- Output of value – i.e. Torque.

It should be noted that for the development as well as implementation purposes a 0-10V range was assumed. This range is easily extended to both positive and negative voltage ranges. This is the case for both input and output, as this is the industry standard that is utilised in the Emotron VFX40-146 variable speed drive for this application.

10.3.1 Input and Data Storage

The Eagle cards utilise a common user developer interface that provides functions to perform specific tasks with the card as well as query the status of the card and process in a variety of ways.

The PCI 730 is capable of performing A/D conversion on 16 channels simultaneously. For this application, initially only one channel is required. The following parameters are specified at the start of the process:

- Sampling Frequency.
- Number of channels to sample.
- Channel.
- File in which data is stored - It should be noted that the data is stored in binary format.
- A software buffer for data values.

The data sampling process is started by calling the functions to start sampling and open the file in which data is stored. The process is ended when the stop sampling and close file functions are called.

10.3.2 Data Input and Units

Torque is expressed in Newton-meters as a function of ω (in radians per second). The measured input from either a tachometer or the analogue output of the VSD itself utilises the 0-10V standard for a speed range of 0-1475 revolutions per minute (r.p.m) being the maximum speed of the induction motor. The voltage input has to be converted to a form that will produce the correct scale of units (i.e. radians per second). For this application the governing equations are then:

10 Volts = 1475 r.p.m therefore 1 volt =147.5 r.p.m

ω (rad/s) = Volts x 147.5 x (2pi/60)…… (1)

Further more it should be noted that the PCI 730 card measures the input voltage in units of microvolts, therefore:

ω (rad/s) = (microvolts x 147.5 x (2pi/60))/1000000……..(2)

This equation represents the relationship between the measured input voltage and rotational speed. It then forms the basis for any further calculations to determine the output torque of the system and the output control voltage.

10.4 Control Algorithm Implementation

The output torque equation as stated previously is:

$$T = J\,(d\omega/dt) + \sum A_n \omega_m$$

The physical variable measured for rotational speed is a 0-10 Volt discrete sampled signal. In this case each discrete sample represents the rotational velocity at that instant in time. The voltage signal is indicated as velocity due to the fact that the polarity of the voltage indicates the direction of rotation.

The method used to determine the derivative of the discrete input signal is Rectangular Approximation [1]. In rectangular approximation the voltage differential dv/dt (if period T is small enough) is approximated by:

$$[v(n) - v(n-1)]/T$$

where v(n) is the nth sample

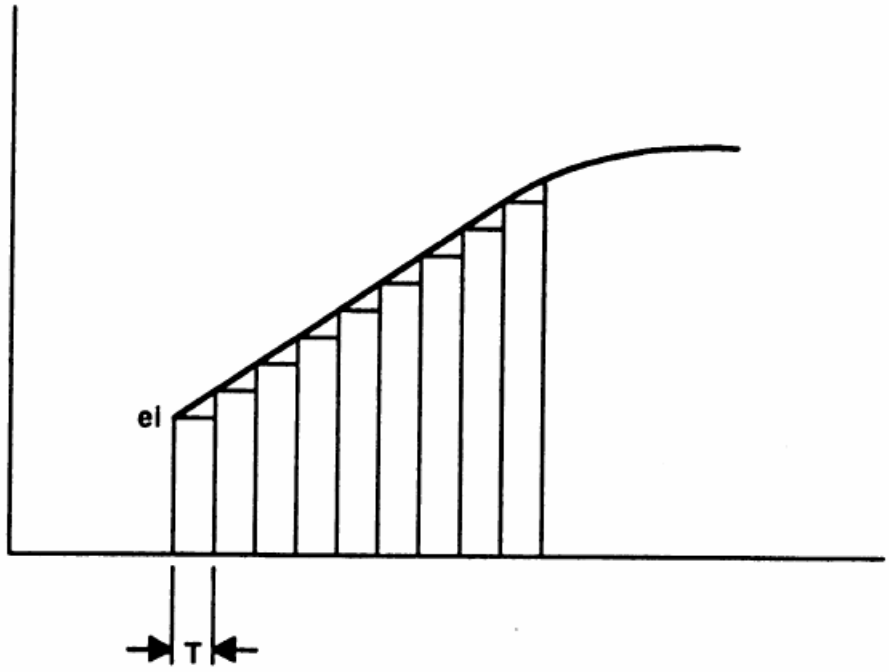

Figure 29: Rectangular approximation [19]

The calculation of the voltage differential is essential in the determination of the dynamic component of the load model for all load types. The voltage derivative determines the rate of change in rotational velocity at any specific instant in time. This component of the model must be accurate and calculated in real-time.

10.4.1 Signal Noise and sensitivity

The problem of signal noise on the analogue signal being received by the A/D card is handled by averaging of samples. The utilisation of single samples leads to sharp changes in the input speed being read due to the presence of noise being generated by both the VSD itself and other external sources. A triangular smoothing average filter is implemented to minimise the influence of random signal noise on the calculated acceleration. The acceleration at any point in time is determined by the subtraction of two averaged speed measurements close together with respect to time so that the differential meets the requirements for accurate rectangular approximation i.e. small period T.

10.4.2 Implementation and Development Issues

The process of developing a program to implement a torque controller comprised the following steps:

10.4.2.1 Familiarisation with Data Acquisition Card and associated software

The Eagle data acquisition cards are provided with a software development kit that interfaces through most of the commonly used programming languages available. The familiarisation process consisted of understanding the functions of the various system calls. This process also included ensuring the learning of the various sampling operations, where the data is stored and the format in which the data is stored.

10.4.2.2 Sampling

The operating system and limitations of the data acquisition card affect the approach taken in utilising the samples from the data card in calculating the voltage differential. The PCI730 card is operated by instructing it to start the sampling process. The data is then written to a hardware buffer in the card. A function call is required to write the data to the software buffer where it can be viewed and accessed. Due to the fact that any function call takes time to process, the sampling frequency is affected if the data is retrieved after each sample. For the control of the process the data is retrieved after a number of samples e.g. 10, 50, 100, 200 etc. This value is pre-set in the system set-up portion of the control code. This sets up a new frequency for the control of the process as the control frequency is then:

Control Frequency = (Sampling Frequency/ (Pre-set Sample Retrieve))

This method in turn necessitates that the card sampling frequency is scaled up to ensure that the control frequency is high enough to implement effective system control.

The user interface allows the selection of the sampling frequency in the range 1-10 kHz. The default sampling frequency is 4 kHz.

10.4.2.3 Motor and VSD Limits

Prevention of damage to the equipment is important for the long-term operation of the programmable load. The safe operation of the drive and motor is ensured by the 0-10V analogue input system of the drive that is matched by the 0-10V output of the A/D card being used.

When the speed of the drive is being controlled by the analogue input, setting the motors maximum operating speed as the limit on the VSD ensures safety. In this case the motor operates at 1475 R.P.M. This then ensures that ±10Volt input from the A/D card equates to ±1475 R.P.M. The acceleration and deceleration in this mode is limited by the

torque limit of the drive. With the brake resistor added to the system, deceleration is limited by the amount of energy that is dissipated by the brake resistor.

With operation in torque mode the motor torque is limited by the maximum torque setting of the VSD, which is entered as a percentage of the motor torque up to a maximum of 400%. For this application, output torque is limited to less than 100% of motor torque in both directions. Limiting system speed in this mode of operation is more complex as a fixed torque applied to an opposing torque that is of smaller magnitude will result in continuous acceleration. Constant speed or steady-state operation is only possible when the opposing forces (torques) are matched in magnitude. The safety limit is ensured by a safety function built into the code that cuts power to the drive and motor if the speed limit is exceeded.

11. USER-INTERFACE

The control program was initially developed as a console format program to establish the basic control loop and functionality of the program. A user-interface design was done on paper to ensure that the input and output parameters matched the functionality of the control program. The Windows interface was developed using Visual C++. The main body of the program was then inserted around the Windows code and modified as required to produce a final working program that interfaced with the variable speed drive and ensured ease of use. The graphical output of data was added to produce graphs that could be saved and re-used by the operator of the programmable load. Access to the data points is also possible in a format that can be copied into Microsoft Excel for analysis and manipulation.

The user interface to configure the load is shown in figure 9.

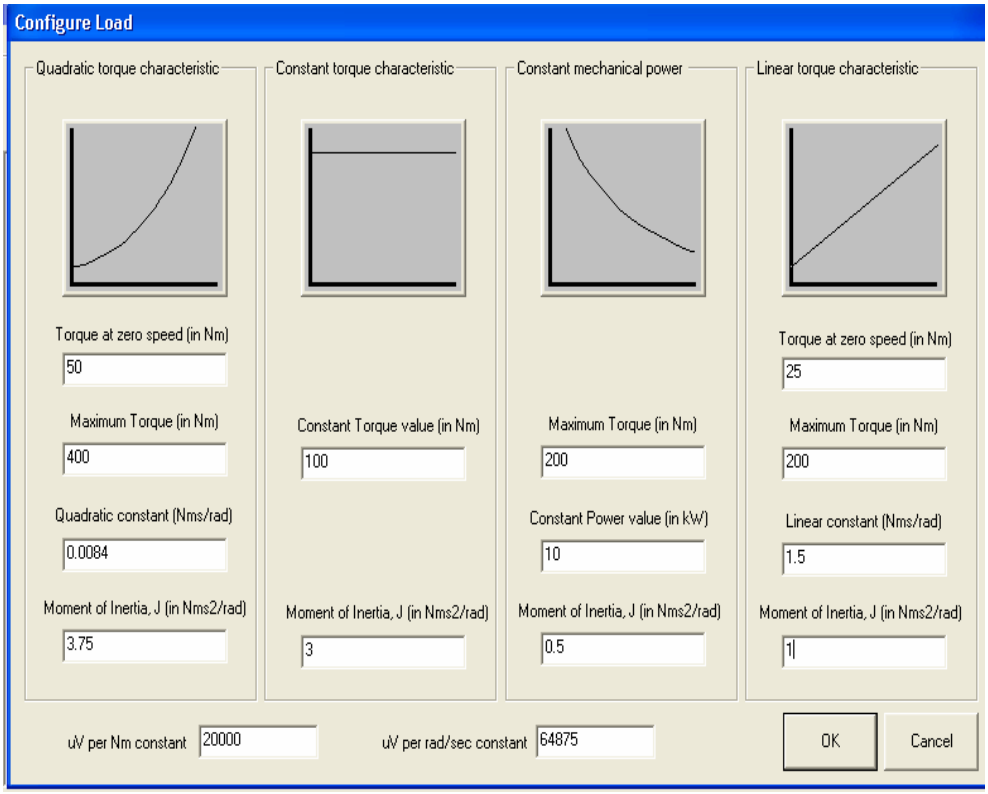

Figure 30: Graphical user-interface for programmable load

The load type is selected via the buttons with the load characteristic icon. The load variables are entered on-screen and can be saved for a specific load that needs to be re-used in other tests. The variables and torque limits that can be set for each load type to specifically describe the load characteristic are shown in table 5.

QUADRATIC TORQUE	**CONSTANT TORQUE**	**CONSTANT POWER**	**LINEAR TORQUE**
Zero Speed Torque	Steady-state Torque	Power	Zero Speed Torque
Maximum Torque	Moment of Inertia	Maximum Torque	Maximum Torque
Quadratic Constant i.e. slope		Moment of Inertia	Linear Constant i.e. slope
Moment of Inertia			Moment of Inertia

Table 5: User-interface programmable parameters

The two constants that can be set by the user at the bottom of the user interface are labelled:

- uV per Nm constant – this value is the ratio between the output voltage (in microvolts) and the torque value in Newton metres. For the 490 Nm motor used to apply the load this ratio is 20408.

- uV per Rad/sec constant – Conversion ratio between the input voltage and speed in radians per second. This value was calculated to be 64875.

The resulting graphs can be saved as Windows metafiles that are easily imported into Microsoft Word documents. The data can also be copied into an Excel file for data manipulation.

12. SYSTEM TESTING

12.1 Steady-State Testing Methodology

The steady state algorithms were tested by varying the speed of a DC motor while the load was applied with an inertia value of zero. The actual torque calculated and applied by the programmable load is compared to the expected value for the specific load equation implemented by the system. This methodology tests the accuracy of the models implemented without the effect that inertia would play during acceleration and deceleration.

12.1.1 Quadratic Torque

The resultant curves from the quadratic torque test are illustrated in figure 31.

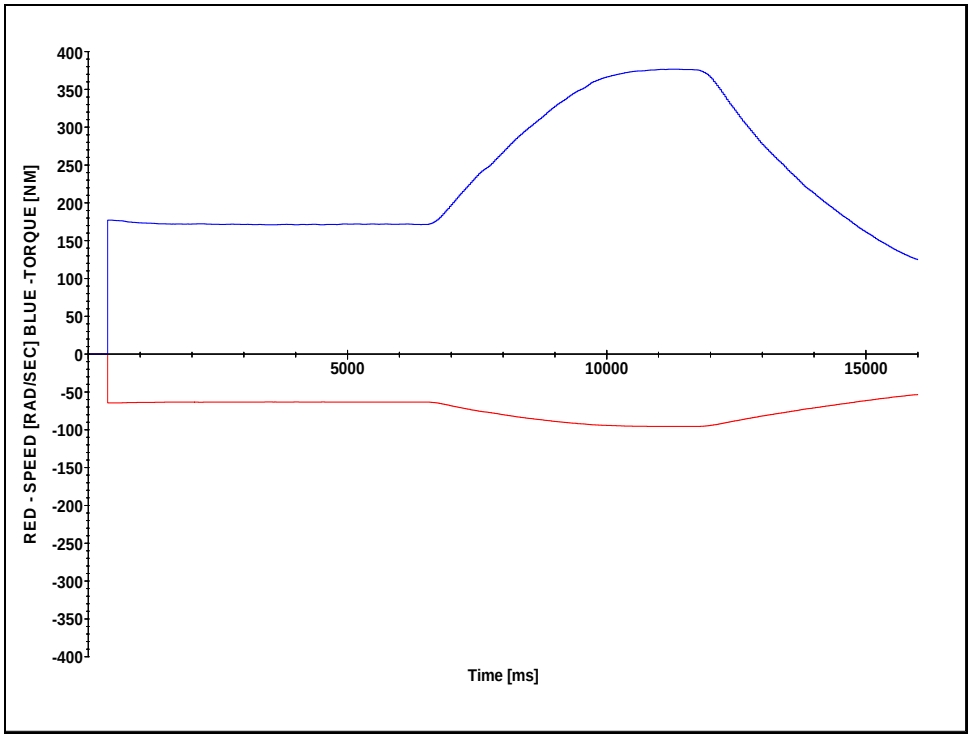

Figure 31: Quadratic Torque Steady-State Response

Random speed points were selected and the actual torque was compared with the expected torque for this speed. The function for this particular torque response is:

$$T = 0.04*\omega^2 + 10$$

Speed is illustrated in red and the resulting torque in blue.

The results for the selected speed points are shown in table 6:

SPEED (RAD/SEC)	EXPECTED TORQUE (NM)	ACTUAL TORQUE (NM)
-63.571	171.651	171.651
-75.563	238.388	238.388
-82.258	280.653	280.652
-95.583	375.441	375.441
-70.282	207.581	207.581

Table 6: Quadratic Torque Steady-State Response

Table 6 shows that the actual output values for torque have an accuracy approaching 100%.

12.1.2 Constant Torque

The resultant curves from the constant torque test are illustrated in figure 32.

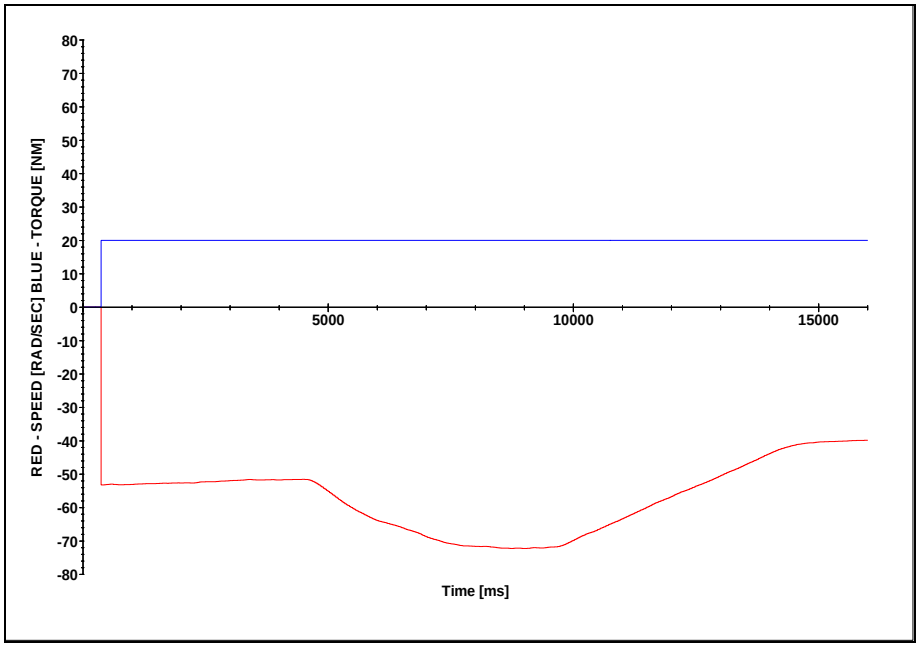

Figure 32: Constant Torque Steady-State Response

Figure 32 illustrates the expected response of no variation in torque as a result of speed variation. Speed is illustrated in red and the resulting torque in blue. Figure 32 indicates the result of a constant torque load with Torque =20Nm.

The results for the selected speed points are shown in table 7:

SPEED (RAD/SEC)	EXPECTED TORQUE (NM)	ACTUAL TORQUE (NM)
-51.9406	20	20
-63.747	20	20
-70.7708	20	20
-65.3357	20	20
-39.8659	20	20

Table 6: Constant Torque Steady-State Response

The steady-state component of this model is completely independent of speed and this is illustrated by table 7 as there is no variation of torque with respect to speed.

12.1.3 Constant Power

The resultant curves from the constant power test are illustrated in figure 33.

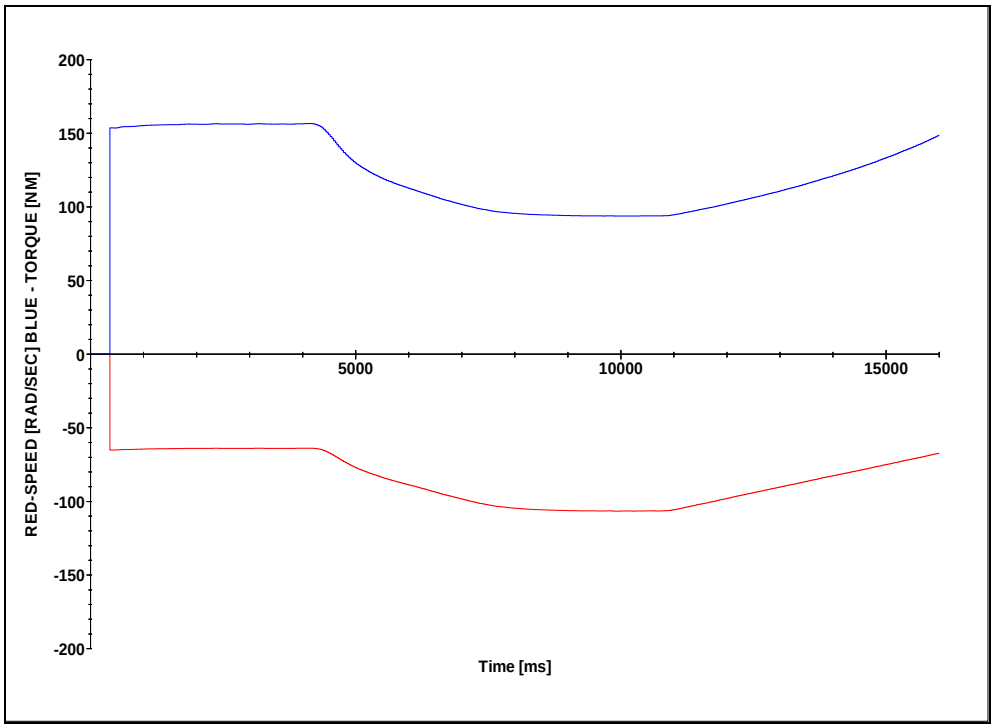

Figure 33: Constant Power Steady-State Response

Figure 33 is the resultant curve for a constant power load with P=10kW. Speed is illustrated in red and the resulting torque in blue. The curve

shows clearly the hyperbolic nature of this function with torque decreasing in magnitude as speed increases in magnitude.

The results for the selected speed points are shown in table 8:

SPEED (RAD/SEC)	EXPECTED TORQUE (NM)	ACTUAL TORQUE (NM)
-65.0976	153.615	153.616
-75.9699	131.631	131.631
-83.3959	119.910	119.910
-106.43	93.958	93.959
-100.92	99.088	99.088

Table 8: Constant Power Steady-State Response

Table 8 shows that the actual output values for torque have an accuracy approaching 100%.

12.1.4 Linear Torque

The resultant curves from the linear torque test are illustrated in figure 34.

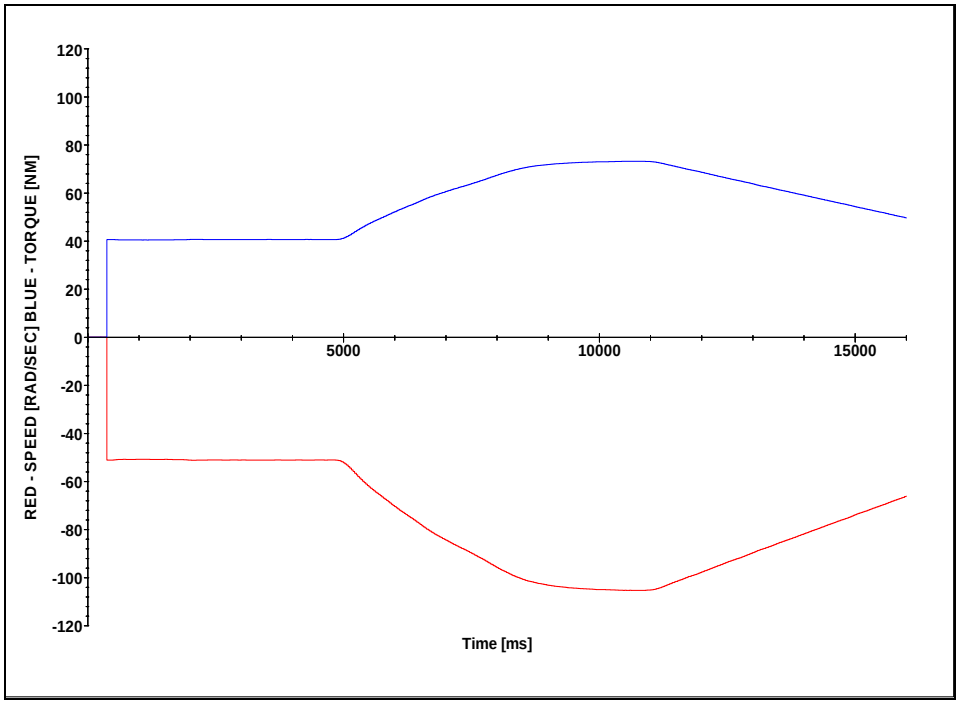

Figure 34: Linear Torque Steady-State Response

The linear torque response for the following function is illustrated in figure 34:

$$T = 0.6*\omega + 10$$

Speed is illustrated in red and the resulting torque in blue. The results for the selected speed points are shown in table 9:

SPEED (RAD/SEC)	EXPECTED TORQUE (NM)	ACTUAL TORQUE (NM)
-51.059	40.635	40.635
-66.4026	49.842	49.842
-80.2088	58.125	58.125
-95.8538	67.512	67.512
-105.288	73.173	73.173

Table 9: Linear Torque Steady-State Response

Table 9 shows that the actual output values for torque have an accuracy approaching 100%.

12.1.5 Results

The steady-state results for all four models tested approach 100% accuracy. This confirms a high level of accuracy for the steady-state models. These models can now be asserted to represent accurate representations of loads under steady-state conditions.

12.2 Dynamic Model Test Methodology (Full Model Test)

The dynamic and complete case (under acceleration or deceleration) was tested by utilising several sections (under dynamic conditions) of the torque and speed curves of differing lengths. The time periods utilised to determine the accuracy of the models are: 1000ms and 100ms. These time periods were specified as they then provide an accuracy level over a relatively short duration event (i.e. 100ms) and a longer duration event (i.e. 1000ms). The comparison was done by:

- Firstly calculating the average acceleration over the time period e.g. 1000ms.
- This value for acceleration was then used to calculate an expected dynamic torque component for evenly spread points in the chosen interval section
- Expected steady-state torque values were also calculated for the specified points.

- The steady-state and dynamic components were summed to produce the expected total torque at that specific point.
- This expected torque was then compared to the actual calculated torque at that instant.
- The **actual** torque is expressed as a percentage of the **expected** torque and this provides a measure of the accuracy of the programmable load.

Note: All units in all tables are as follows: Speed – rad/s, acceleration - rad/s^2, torque – Nm.

12.2.1 Quadratic Torque

The model tested against for the quadratic load was the following:

$$T = 2\frac{d\omega}{dt} + 0.07\omega^2 + 20$$

The resulting speed and torque curves are shown in figure 35.

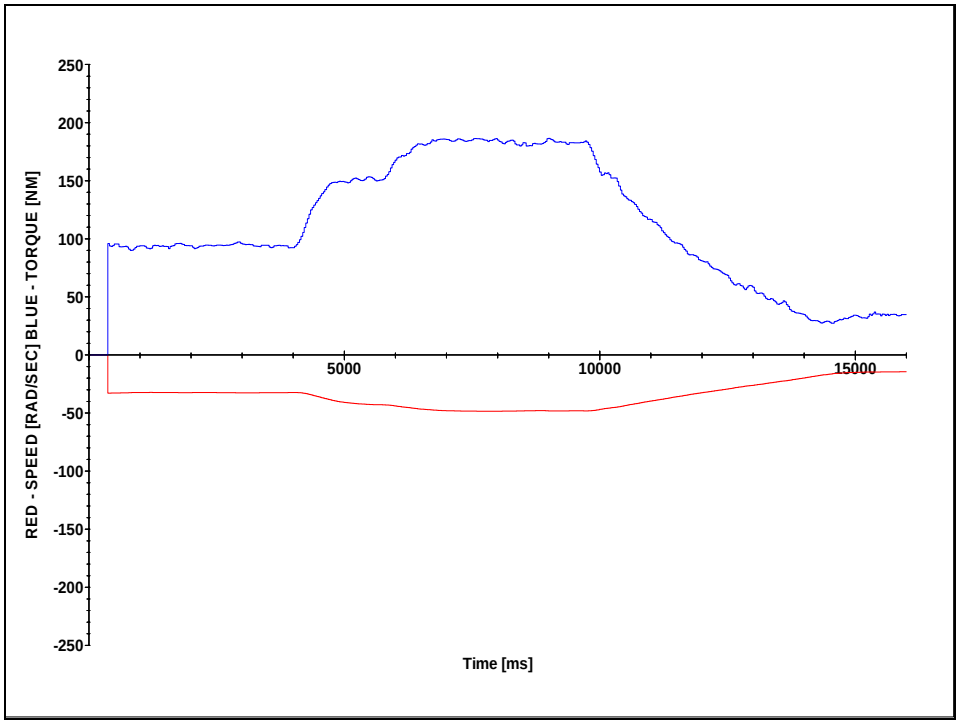

Figure 35: Quadratic Torque Response

1000MS TEST CASE

The portion tested is the time period 11000ms to 12000ms which falls under the deceleration portion of the speed curve (red). Table 10 displays the speed, torque and average acceleration over this period.

TIME	SPEED	TORQUE
11000	-39.669	**116.575**
12000	-32.523	**80.869**
AVERAGE ACCELERATION	7.146 rad/s^2	

Table 10: Average acceleration 1000ms - Quadratic

The results for the time points in between are detailed in table 11.

Time (ms)	**11100**	**11300**	**11500**	**11700**	**11900**
SPEED	-39.05	-37.666	-35.984	-34.68	-33.367
Actual Torque	**114.076**	**103.471**	**96.48**	**89.365**	**85.181**
STEADY-STATE TORQUE	106.742	99.313	90.638	84.188	77.935
DYNAMIC TORQUE	**14.292**	**14.292**	**14.292**	**14.292**	**14.292**
CONSTANT	20	20	20	20	20
TOTAL EXPECTED TORQUE	**112.45**	**105.021**	**96.346**	**89.896**	**83.643**
ACTUAL TORQUE AS % OF EXPECTED TORQUE	**101.45**	**98.52**	**100.14**	**99.41**	**101.84**

Table 11: Comparison of expected vs. actual torque (1000ms) - Quadratic

Table 11 shows that the actual torque as a percentage of expected torque at each of the 5 specified time points in the 1000ms window is within 2% of the expected torque.

100MS CASE

The portion tested is the time period 11450ms to 11550ms. Table 12 displays the speed, torque and average acceleration over this period.

TIME	SPEED	TORQUE
11450	-36.4285	97.2051
11550	-35.7713	96.0927
AVERAGE ACCELERATION	6.572 rad/s^2	

Table 12: Average acceleration 100ms- Quadratic

The results for the midway point are detailed in table 13:

Time (ms)	**11450**	**11500**	**11550**
SPEED	-36.4285	-35.9837	-35.7713
Actual Torque	97.2051	**96.48**	96.0927
STEADY-STATE TORQUE		90.638	
DYNAMIC TORQUE		**13.144**	
CONSTANT		20	
TOTAL EXPECTED TORQUE		**97.494**	
ACTUAL TORQUE AS % OF EXPECTED TORQUE		**98.96**	

Table 13: Comparison of expected vs. actual torque (100ms) - Quadratic

A comparison has been made of expected torque vs. averaged torque over various time periods during the dynamic state of motion. This was done for time periods 100ms and 1000ms. The actual torque was within 2% of the expected torque for both the tested periods. An accuracy of 2 % is deemed to be acceptable for this application.

12.2.2 Constant Power

The model tested against for the quadratic load was the following:

$$T = \frac{10000}{\omega} + \frac{d\omega}{dt}$$

This is equivalent to a 10kW load, with the maximum torque in this particular case is set at 400Nm.

The demonstrated torque and speed curves are illustrated in figure 36.

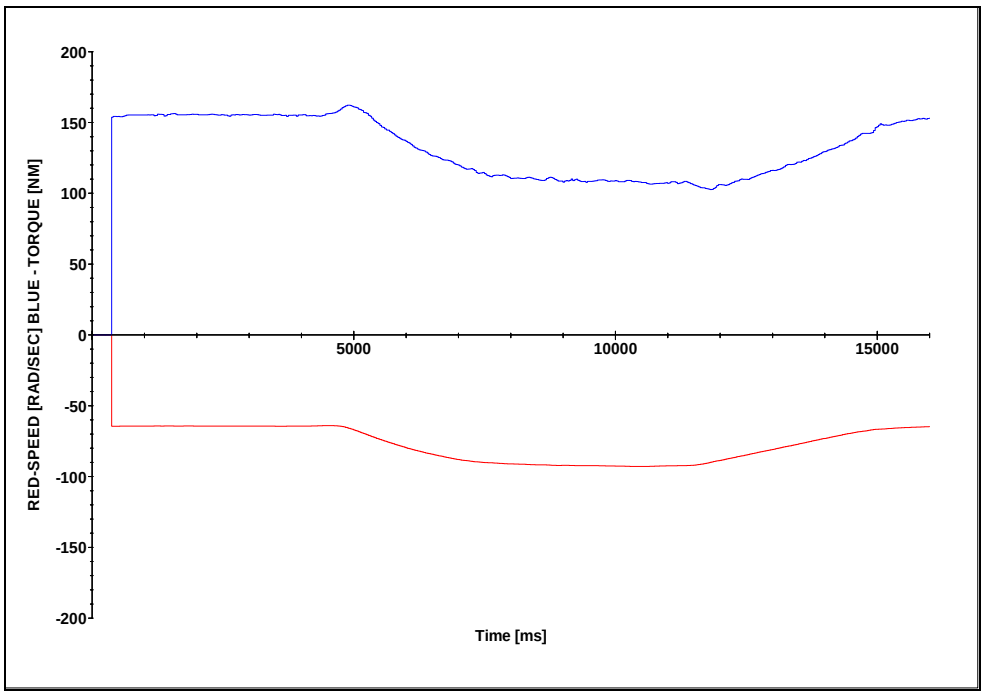

Figure 36: Constant Power Response

1000MS TEST CASE

The portion tested is the time period 5000ms to 6000ms which falls under one of the dynamic portions of the speed curve (red). Table 14 displays the speed, torque and average acceleration over this period.

TIME (ms)	SPEED	TORQUE
5000	-67.1337	160.927
6000	-79.7483	136.58
AVERAGE ACCELERATION	-12.615	

Table 14: Average acceleration 1000ms – Constant Power

The results for the selected time points in between are detailed in table 15.

Time (ms)	**5100**	**5300**	**5500**	**5700**	**5900**
SPEED	-68.374	-71.012	-73.875	-76.185	-78.347
Actual Torque	159.282	155.056	147.886	143.646	138.839
STEADY-STATE TORQUE	146.255	140.822	135.363	131.259	127.637
DYNAMIC TORQUE	-12.615	-12.615	-12.615	-12.615	-12.615
CONSTANT	0	0	0	0	0
TOTAL EXPECTED TORQUE	158.87	153.436	147.978	143.874	140.251
ACTUAL TORQUE AS % OF EXPECTED TORQUE	**100.26%**	**101.06%**	**99.94%**	**99.84%**	**98.99%**

Table 15: Comparison of expected vs. actual torque (1000ms) – Constant Power

Table 15 shows that the actual torque as a percentage of expected torque at each of the 5 specified time points in the 1000ms window falls largely within 1% of the expected torque. This is the case for all but one of the test points for, for which it falls within 1.1% of the expected torque

100MS CASE

The portion tested is the time period 12950ms to 13050ms. Table 16 displays the speed, torque and average acceleration over this period.

TIME (ms)	SPEED	TORQUE
12950	-81.3999	115.529
13050	-80.6651	116.063
AVERAGE ACCELERATION	7.348	

Table 16: Average acceleration 100ms- Constant Power

The results for the midway point are detailed in table 17:

Time (ms)	**12950**	**13000**	**13050**
SPEED	-81.3999	-80.9267	-80.6651
Actual Torque	115.529	116.124	116.063
STEADY-STATE TORQUE	122.85	123.569	123.969
DYNAMIC TORQUE	7.348	7.348	7.348
CONSTANT		0	
TOTAL EXPECTED TORQUE		116.221	
ACTUAL TORQUE AS % OF EXPECTED TORQUE		**99.92%**	

Table 17: Comparison of expected vs. actual torque (100ms) – Constant Power

Table 17 shows that the actual torque as a percentage of expected torque at the midway point of the 100ms window falls within 0.1% of the expected torque.

12.2.3 Constant Torque

The model tested against for the constant torque load was the following:

$$T = 20 + \frac{d\omega}{dt}$$

The resulting speed and torque curves are shown in figures 37.

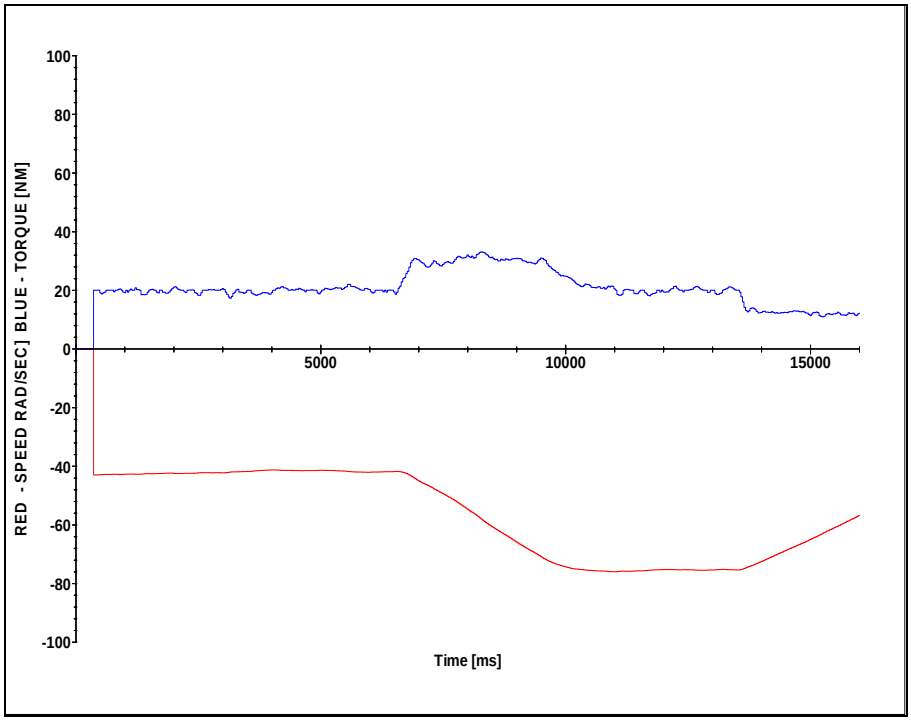

Figure 37: Constant Torque Response

1000MS TEST CASE

The portion tested is the time period 8000ms to 9000ms. Table 18 displays the speed, torque and average acceleration over this period.

TIME (ms)	SPEED	TORQUE
8000	-54.6441	32.0245
9000	-65.8519	30.9328
AVERAGE ACCELERATION	-11.208	

Table 18: Average acceleration 1000ms- Constant Torque

The results for the selected time points in between are detailed in table 19.

Time (ms)	**8100**	**8300**	**8500**	**8700**	**8900**
SPEED	-55.6952	-58.4124	-60.6005	-62.5377	-64.8187
Actual Torque	31.675	32.994	31.337	30.603	30.665
STEADY-STATE TORQUE	20	20	20	20	20
DYNAMIC TORQUE	-11.208	-11.208	-11.208	-11.208	-11.208
CONSTANT	0	0	0	0	0
TOTAL EXPECTED TORQUE	31.208	31.208	31.208	31.208	31.208
ACTUAL TORQUE AS % OF EXPECTED TORQUE	101.50%	105.72%	100.41%	98.06%	98.26%

Table 19: Comparison of expected vs. actual torque (1000ms) – Constant Torque

Table 19 shows that the actual torque as a percentage of expected torque at each of the 5 specified time points in the 1000ms window is within 2% of the expected torque.

100MS CASE

The portion tested is the time period 12950ms to 13050ms. Table 20 displays the speed, torque and average acceleration over this period.

TIME (ms)	SPEED	TORQUE
14500	-68.7081	12.451
14600	-68.0083	12.717
AVERAGE ACCELERATION	6.998	

Table 20: Average acceleration 100ms- Constant Torque

Time (ms)	14500	14550	14600
SPEED	-68.7081	-68.2471	-68.0083
Actual Torque	12.451	12.6479	12.7171
STEADY-STATE TORQUE	20	20	20
DYNAMIC TORQUE		6.998	
CONSTANT		0	
TOTAL EXPECTED TORQUE		13.002	
ACTUAL TORQUE AS % OF EXPECTED TORQUE		97.28%	

Table 21: Comparison of expected vs. actual torque (100ms) – Constant Torque

Table 21 shows that the actual torque as a percentage of expected torque at the midway point of the 100ms window falls within 3% of the expected torque.

12.2.4 Linear Torque

The model tested against for the linear torque load was the following:

$$T = 0.5\omega + \frac{d\omega}{dt} + 10$$

The resulting speed and torque curves are shown in figure 38.

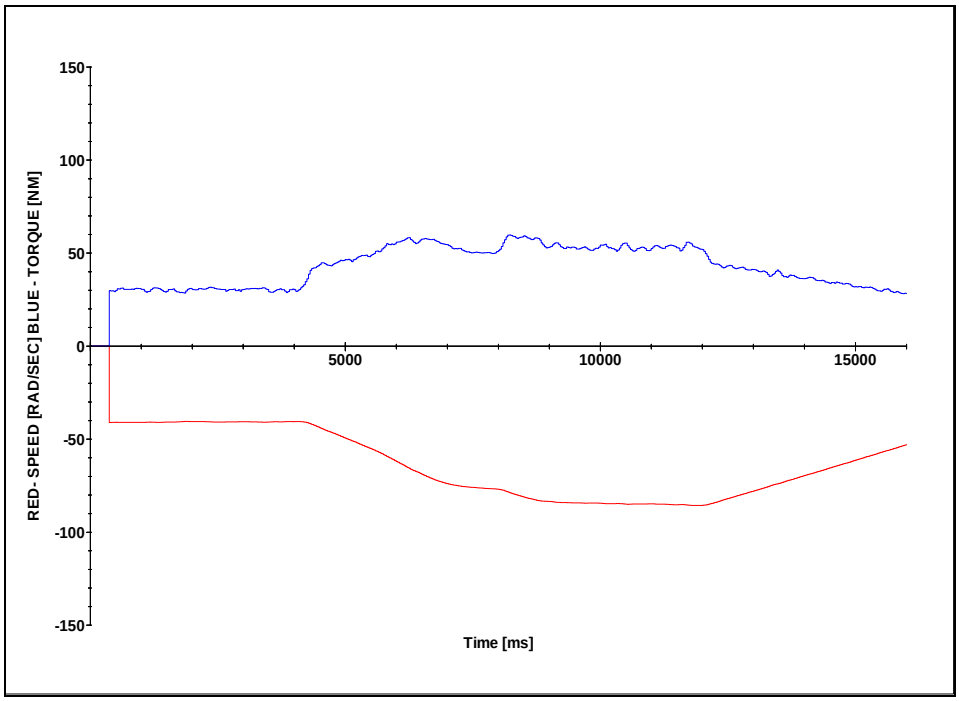

Figure 38: Linear Torque Response

1000MS TEST CASE

The portion tested is the time period 5000ms to 6000ms which falls under one of the dynamic portions of the speed curve (red). Table 22 displays the speed, torque and average acceleration over this period.

TIME (ms)	SPEED	TORQUE
5000	-49.5031	46.5016
6000	-61.9895	55.8329
AVERAGE ACCELERATION	-12.4864	

Table 22: Average acceleration 1000ms- Linear Torque

The results for the selected time points in between are detailed in table 23.

Time (ms)	**5100**	**5300**	**5500**	**5700**	**5900**
SPEED	-50.538	-52.6577	-55.1515	-57.463	-60.1869
Actual Torque	46.1023	48.1784	48.8187	51.078	54.4613
STEADY-STATE TORQUE	25.269	26.329	27.576	28.732	30.093
DYNAMIC TORQUE	-12.486	-12.486	-12.486	-12.486	-12.486
CONSTANT	10	10	10	10	10
TOTAL EXPECTED TORQUE	47.755	48.815	50.062	51.218	52.58
ACTUAL TORQUE AS % OF EXPECTED TORQUE	96.54%	98.70%	97.52%	99.73%	103.58%

Table 23: Comparison of expected vs. actual torque (1000ms) – Linear Torque

Table 23 shows that the actual torque as a percentage of expected torque at each of the 5 specified time points in the 1000ms window is within 3.5% of the expected torque.

100MS CASE

The portion tested is the time period 12950ms to 13050ms. Table 24 displays the speed, torque and average acceleration over this period.

TIME (ms)	SPEED	TORQUE
13900	-70.6199	36.6092
14000	-69.5377	36.2696
AVERAGE ACCELERATION	10.822	

Table 24: Average acceleration 100ms- Linear Torque

Time (ms)	13900	13950	14000
SPEED	-70.6199	-70.0689	-69.5377
Actual Torque	36.6092	36.3157	36.2696
STEADY-STATE TORQUE	35.31	35.034	34.769
DYNAMIC TORQUE		10.822	
CONSTANT		10	
TOTAL EXPECTED TORQUE		34.212	
ACTUAL TORQUE AS % OF EXPECTED TORQUE		106.15%	

Table 25: Comparison of expected vs. actual torque (100ms) – Linear Torque

The results for the linear model are the worst of the four models tested. This result is still only 6.15% over the expected target.

The testing provides a snapshot that gives an indication of the accuracy levels that can be expected from the programmable load. The dynamic testing of the four load type models all returned results with a level of well within 10% of the expected value. This level of accuracy is deemed acceptable as at present dynamic conditions have only been modelled by the addition of flywheel weights on a spinning rotor to create inertia.

12.3 Acceleration Limits

12.3.1 Maximum Acceleration

The maximum acceleration limits of the system were tested by setting the variable speed drive torque limits to maximum and running the drive under no load. This represents the maximum acceleration that the variable speed drive would be able to produce. Acceleration and speed curves were plotted.

The following curves were plotted:

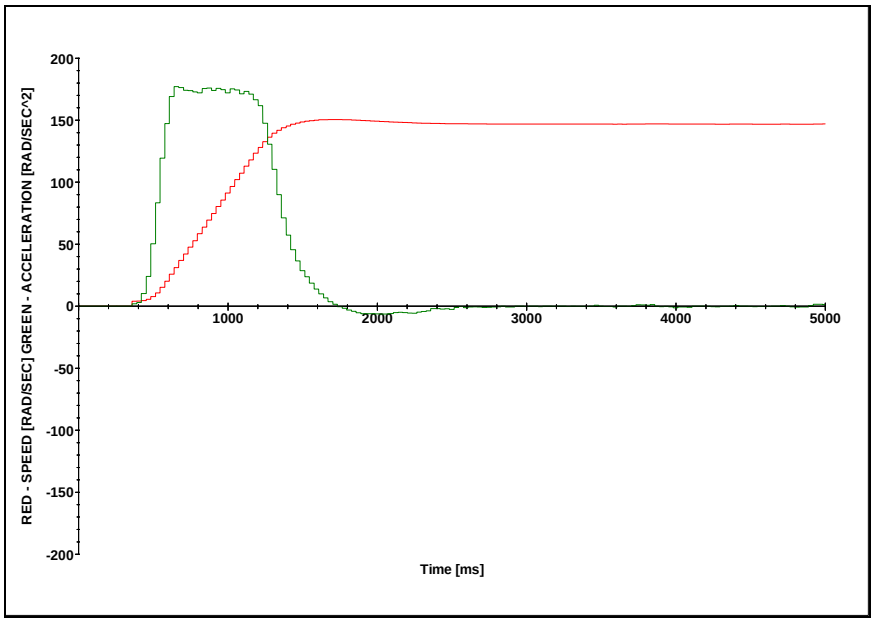

Figure 39: Maximum Acceleration and Speed

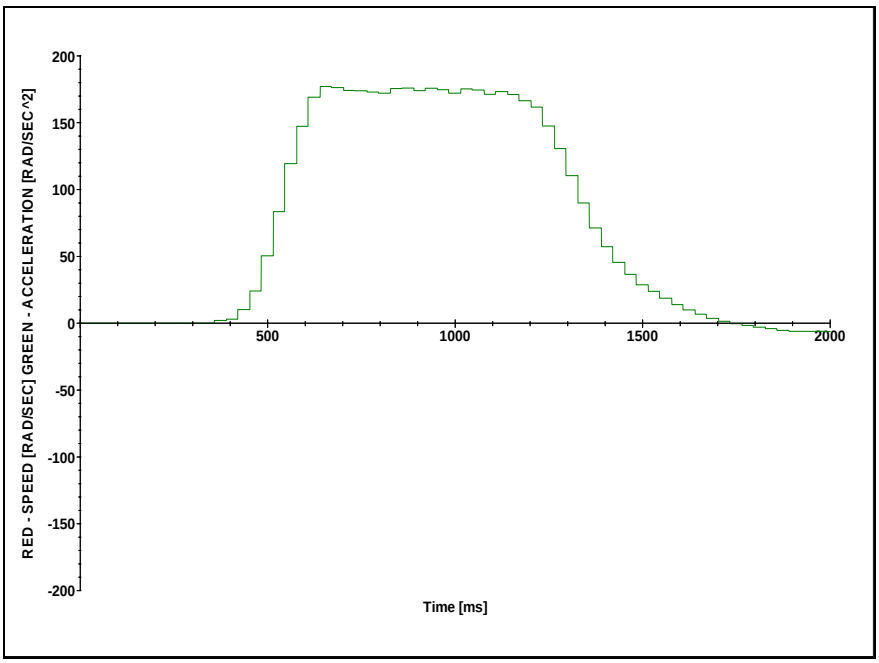

Figure 40: Acceleration Curve

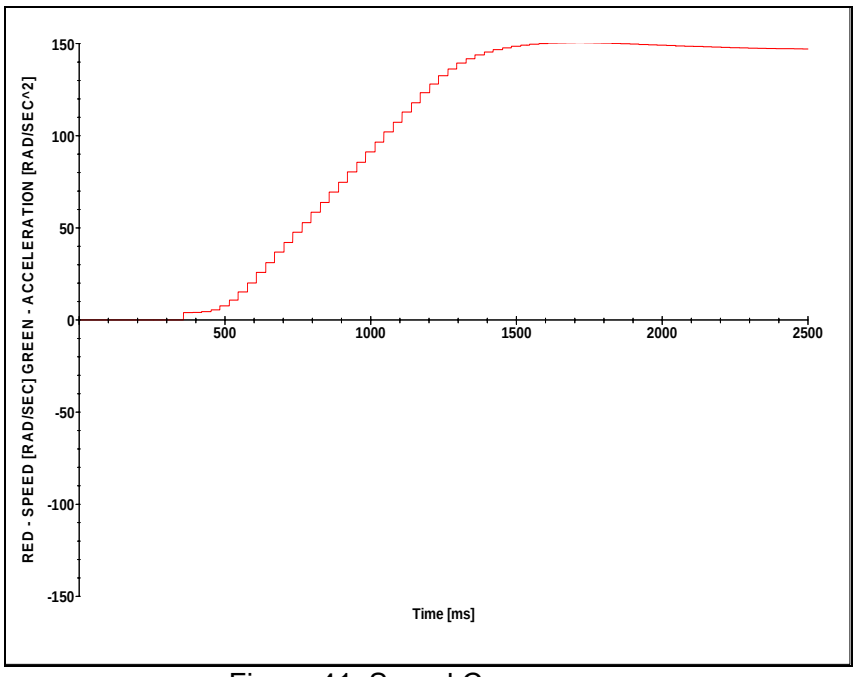

Figure 41: Speed Curve

Figures 39, 40 and 41 show the acceleration and speed plots for the maximum acceleration test. The maximum acceleration achieved by the motor was 150.493 rad/s^2. This is then recognised as being the maximum acceleration limit of the programmable load.

12.3.2 Minimum Acceleration

The dynamic calculation of torque utilised in the programmable load is dependent on the calculated acceleration. The minimum valid acceleration at which a representatively accurate dynamic component of torque can be calculated is a key aspect of this. Due to the high levels of accuracy in modelling the output torque for both transient and steady state conditions it became apparent during testing that minor fluctuations in speed are translated onto the output torque signal. These are introduced as a result of minor vibrations on the rotor shaft. Smoothing of the signal was introduced as a countermeasure to this. This was done by means of introducing a deadband around the zero acceleration point.

The key issues around this are:

- Minor changes/fluctuations in the steady-state speed as a result of noise on speed signal or minor mechanical fluctuations e.g. slight shaft vibration
- The stage at which a low acceleration level is considered to be steady state

The level of the deadband was set around these two criteria.

The net result of minor fluctuations is typically just a noisy signal which distorts the output torque calculation but in most cases has no significant impact on the system torque. It may in cases with high inertia loading result in a significant impact on the system. The impact this would have on a rotor shaft should also then be taken into consideration and in all likelihood minor vibrations would be minimal under these conditions.

The introduction of a deadband directly influences the sensitivity of the system. Essentially if the deadband is set too high, calculations based on transient conditions with small fluctuations cannot be done and if it is set too low, minor environmental and noise elements influence the output results.

The key application of the programmable load is the modelling of mechanical loading under voltage dip conditions. According to NRS-048 the maximum duration of a dip is 3 seconds. The minimum variation in speed over this time range then becomes a key criterion for the deadband limit.

The process sensitivity to speed then becomes a consideration; this varies from industry to industry with the paper and pulp industry being particularly sensitive. Using the 3 second criteria of NRS-048 to establish a deadband limit based on deceleration from the maximum point, table 26 shows the maximum potential for speed change in a single direction over a one to three second interval at lower levels of acceleration/ deceleration. The assumed process speed is 1400 R.P.M.

Process Speed (RPM)	**1400**	**1400**	**1400**	**1400**	**1400**
acceleration rate (rad/s^2)	2.5	1.5	1	0.75	0.5
RPM Change Per Second	23.89	14.31	9.52	7.17	4.78
Resultant Speed after 1 second (R.P.M)	1376.11	1385.69	1390.48	1392.83	1395.22
% Speed Change	**1.71%**	**1.02%**	**0.68%**	**0.51%**	**0.34%**
R.P.M Change for 3 seconds	71.66	42.94	28.55	21.50	14.33
Resultant Speed after 3 seconds (R.P.M)	1328.34	1357.06	1371.45	1378.50	1385.67
% Speed Change	**5.12%**	**3.07%**	**2.04%**	**1.54%**	**1.02%**

Table 26: Speed Changes over a 3 second interval at low levels of acceleration

Table 26 illustrates that for the maximum considered deadband level of 2.5 rad/s^2, a process speed change of 5.12% is the result. These figures were taken into account when considering the practicality of implementing the deadband. Through a process of trial and error the resulting deadband level decided on was 1.5 rad/s^2. For a system with a process speed of 1400 R.P.M, the sensitivity over a 3 second interval at low acceleration is 3.07%. Simply, the system will register all outputs below 3.07% speed change as zero.

13. CONCLUSIONS AND RECOMMENDATIONS

13.1 Conclusions

Industrial load types were investigated and three major categories were identified: constant torque, constant power and variable torque. It has been shown that these load types together with load inertia affect the voltage dip performance of variable speed drives.

The load characteristics are modelled according to torque vs. speed equations. The equations for the three prevalent load types were identified and stated. These equations form the basis for the modelling of various industrial loads.

It was identified that modelling of industrial loads is essentially the control of the opposing torque seen by the equipment under test (specifically at the motor shaft).

Field-oriented control of an induction motor was identified as an accurate, high-speed method of producing an opposing torque. The equations describing the control of an induction motor were developed and a control strategy illustrated.

An implementation method for the development of the programmable load was suggested with required equipment specified and a control algorithm developed.

The programmable load has been constructed and the associated software developed according to the implementation method. System tests were conducted and the accurate operation of the load under steady state and dynamic conditions was confirmed. The accuracy of the calculated output torque values and output voltage of the programmable load was verified utilising average acceleration to calculate torque over two time periods (i.e. 100ms and 1000ms). This testing was done to provide an indication of the expected accuracy of the load models as

executed by the programmable load. The worst case accuracy calculated during testing was 106.15% utilising the linear torque load.

The maximum acceleration limit was established at 150.493 rad/s^2 and a minimum acceleration deadband limit set at 1.5 rad/s^2.

The development and implementation of the programmable load with a maximum torque output of 400Nm that can simulate quadratic, constant and linear torque loads as well as constant power loads, under steady-state and transient conditions has been completed.

13.2 Recommendations

The following recommendation is made:

- The programmable load should be utilised in the voltage dip testing of variable speed drives to quantify the impact of both load type and inertia on the dip performance of these drives.

REFERENCES

[1] Koch RG, *"Dip Design Considerations: Plant Dip Mitigation Design Guideline"*, Eskom Research Report, RES/RR/99/00042, December 1999

[2] Abrahams RW, *"Voltage Dip Compatibility Testing for Variable Speed Drives"*, MSc Thesis, Robin Abrahams, University of the Witwatersrand, September 2000.

[3] Langley R, Mansoor A, Fortenbery B, Cooke T, *"Evaluation of Ride-Through*. *Systems for Adjustable-Speed Drives*", TR-111952, EPRI, Palo Alto, CA, November 1998

[4] Abrahams RW, Van Coller J, *"Voltage Dip Testing of Auxilliary Plant Equipment",* Eskom research report, No. RES/RR/01/15089, December 2001

[5] NRS048-1: 1996, *"Electricity Supply – Quality of Supply Part 1: Overview of implementation of standards and procedures – for application in the Electricity Supply Industry"* First Edition, 1996. Amendment 1, 1998.

[6] NRS048-2: 1996, *"Electricity Supply – Quality of Supply Part 2: Minimum Standards – for application by the National Electricity Regulator"*, First Edition, 1996. Amendment 1, 1998.

[7] DRAFT IEEE Standard 1159.2: (draft) *"Recommended Practice for the Characterization of a Power Quality Event"*, 1996.

[8] Raj Narayanan, Don Platt, Sarath Perera, "*Improvements To Voltage Sag Ride-Through Performance Of AC Variable Speed Drives"*, Integral Energy Power Quality Centre, School of Electrical, Computer and Telecommunications Engineering, University of Wollongong

[9] A Mansoor, T Key, B Moncrief, *"Disruption of Industrial Process Controls by Voltage Sags"* Proceedings: 8th International Power Quality Applications Conference, PQA, Cape Town, South Africa, November 9-11, 1998

[10] Mansoor A, Collins Jr. E.R, Morgan R.L, *"Effects of Unsymmetrical Voltage Sags adjustable Speed Drives"*, http://ece.clemson.edu/power/pqia/pdfs/Sag1ph.pdf Last accessed October 2002

[11] Langley R, Mansoor A, Fortenbery B, Cooke T, *"Evaluation of Ride-Through Systems for Adjustable-Speed Drives*", TR-111952, EPRI, Palo Alto, CA, November 1998.

[12] "What is torque?" Course notes: Department of Physics, University of Guelph http://www.physics.uoguelph.ca/tutorials/torque/Q.torque.intro.html, Last accessed October 2002.

[13] Cowern E., *"Understanding Torque"*, The Cowern Papers, www.motorsanddrives.com, last accessed October2002

[14] Serway R, *"Physics for Scientists and Engineers, 4th Ed."*, Saunders College Publishing, Florida, 1996

[15] Abrahams RW, Van Coller JM, "*Using a new protocol with the voltage dip testing of a 30 KVA DC drive"* Eskom research report No. RES/RE/00/11435, November 2000.

[16] Texas Instruments Europe, *"Field Oriented Control of 3-Phase AC Motors"*, February 1998.

[17] Van Coller JM, *"Variable Speed AC Machine Drives"*, Course Notes ELEN 599, University of the Witwatersrand, 1999.

[18] Emotron, "*VECTORFLUX VFB/VFX Instruction Manual*", Supplied with the Emotron VFX40-146 VSD by Saftronics South Africa.

[19] Irfan Ahmed, *"Implementation of PID and Deadbeat Controllers with the TMS320 Family"*, Texas Instruments Application Report SPRA 083, www.ti.com, Last accessed June 2003.

[20] Eagle Technology, "P*CI730 User Manual"*, www.eagledaq.com, Last accessed September 2004.

APPENDIX A: IMPLEMENTATION CIRCUIT DIAGRAM